New Synthetic Routes to Azacarborane Clusters: Nitrile Insertion Reactions of *nido*-5,6-$C_2B_8H_{11}^-$ and *nido*-$B_{10}H_{13}^-$

Andrew E. Wille, Kai Su, Patrick J. Carroll, and Larry G. Sneddon*

Contribution from the Department of Chemistry, University of Pennsylvania, Philadelphia, Pennsylvania 19104-6323

Received March 11, 1996[⊗]

Abstract: A synthetic sequence involving the initial nucleophilic attack of the isoelectronic *nido*-5,6-$C_2B_8H_{11}^-$ or *nido*-$B_{10}H_{13}^-$ anions at a nitrile carbon, followed by nitrile hydroboration and cage-insertion, has been found to yield new azacarborane clusters in good yields. Thus, the reaction of *nido*-5,6-$C_2B_8H_{11}^-$ with refluxing acetonitrile gave the azatricarbaborane anion *arachno*-7-CH_3-5,7,14,12-$C_3NB_8H_{11}^-$ (**1**$^-$) in 65% yield, while *nido*-$B_{10}H_{13}^-$ reacted with acetonitrile, benzyl cyanide, or $CH_3{}^{13}CN$ to give the azamonocarbaborane anions *arachno*-7-CH_3-7,12-$CNB_{10}H_{13}^-$ (**2a**$^-$), *arachno*-7-Bn-7,12-$CNB_{10}H_{13}^-$ (**2b**$^-$), and *arachno*-7-CH_3-7,12-$^{13}CNB_{10}H_{13}^-$ (**2a**$^-$-^{13}C), respectively. Single-crystal X-ray studies of the isoelectronic clusters, **1**$^-$ and **2a**$^-$, showed that hydroboration of the nitrile occurred, with the resulting imino group inserting into the cage framework in a position bridging the B2 and B11 borons. Consistent with their arachno skeletal electron counts, **1**$^-$ and **2a**$^-$ have cage frameworks containing two six-membered open faces that may be derived from a bicapped hexagonal antiprism by removal of two non-adjacent five-coordinate vertices. Alternatively, **1**$^-$ and **2a**$^-$ may be considered as having 10-vertex arachno frameworks with exopolyhedral bridging imine substituents. Acidification of **1**$^-$ resulted in loss of one boron and the imine nitrogen and formation of the known tricarbaborane *nido*-6-CH_3-5,6,9-$C_3B_7H_{10}$. In contrast, acidification of **2**$^-$ led to loss of only one boron to yield the new azamonocarbaborane *hypho*-12-R-12,13-CNB_9H_{15} (**3**). A single-crystal X-ray study confirmed that **3** has an 11-vertex hypho structure, containing two six-membered open faces, that is based on a 14-vertex closo polyhedron missing three vertices. In **3**, further hydroboration of the CN group occurred, such that the carbon contains an additional hydrogen and the nitrogen is connected to two borons. Deprotonation of **3** with Proton Sponge, 1,8-bis(dimethylamino)naphthalene, initially yielded *hypho*-12-R-12,13-$CNB_9H_{14}^-$ (**3**$^-$), which subsequently underwent a skeletal rearrangement to yield the isomeric anion *hypho*-12-R-12,11-$CNB_9H_{14}^-$ (**4**$^-$). A single-crystal X-ray study of **4**$^-$ confirmed that it has an 11-vertex hypho structure with one seven-membered and one five-membered open face. Subsequent acidification of **4**$^-$ resulted in loss of one additional boron to give *hypho*-8-R-8,13-CNB_8H_{14} (**5**). Deprotonation with Proton Sponge gave the new anion *hypho*-8-R-8,13-$CNB_8H_{13}^-$ (**5**$^-$). Based upon spectral and computational data, **5** and **5**$^-$ are proposed to have the CN unit incorporated into a 10-vertex hypho structure.

Introduction

The syntheses, structures, and chemistry of hybrid clusters, such as the polyhedral azacarboranes, containing both electron-deficient and electron-rich cage atoms, are of continuing interest in polyhedral cluster chemistry since these clusters may show bonding and structural properties intermediate with those of the classical and nonclassical cluster classes. Although several azaboranes[1] and metallaazaboranes[2] have recently been reported, there remain only a few azacarborane clusters, *nido*-7,8,10-$C_2NB_8H_{11}$,[3] *arachno*-$\mu_{8,9}$-NH_2-5,6-$C_2B_8H_{11}$,[3] *arachno*-11-Bu^t-5,10,11-$C_2NB_8H_{12}$,[4] and *arachno*-6,9-CNB_8H_{13}.[5] These azacarboranes have been synthesized employing reagents such as nitrous acid, NH_2Bu^t or sodium nitrite, giving yields ranging from 15 to 68%. Thus, general efficient synthetic routes to azacarboranes have not yet been developed.

We have previously reported[6] that the carbon atoms in nitriles are susceptible to nucleophilic attack by certain polyhedral thiaborane and carborane anions and that such reactions lead to either CN or carbon insertion reactions, producing new thiaazacarboranes or tricarbaboranes. Thus, the reaction of acetonitrile with *arachno*-6,8-$S_2B_7H_8^-$ results in CN insertion to give *hypho*-5-CH_3-5,11,7,14-$CNS_2B_7H_9$ (eq 1) while the reaction of the isoelectronic carborane anion *arachno*-6,8-$C_2B_7H_{12}^-$ with acetonitrile results in carbon insertion to yield *nido*-6-CH_3-5,6,9-$C_3B_7H_{10}$ (eq 2).

$$\textit{arachno}\text{-}6,8\text{-}S_2B_7H_8^- + CH_3CN \xrightarrow[(2)\ H^+]{(1)\ \text{reflux}} \textit{hypho}\text{-}5\text{-}CH_3\text{-}5,11,7,14\text{-}CNS_2B_7H_9 \quad (1)$$

$$\textit{arachno}\text{-}6,8\text{-}C_2B_7H_{12}^- + CH_3CN \xrightarrow[(2)\ H^+]{(1)\ \text{reflux}} \textit{nido}\text{-}6\text{-}CH_3\text{-}5,6,9\text{-}C_3B_7H_{10} + NH_3 \quad (2)$$

These results suggested that borane-anion/nitrile reactions might provide general routes to a variety of new azacarborane and/or carborane clusters. Indeed, in this paper, we report our synthetic and structural studies of a variety of such clusters that have resulted from the reactions of nitriles with the isoelectronic anions, *nido*-5,6-$C_2B_8H_{11}^-$ and *nido*-$B_{10}H_{13}^-$.

Experimental Section

All manipulations were carried out by using standard high vacuum or inert-atmosphere techniques as described by Shriver.[7]

Materials. Decaborane, $B_{10}H_{14}$, was obtained from laboratory stock and sublimed before use. The carborane, *nido*-5,6-$C_2B_8H_{12}$, and its anion were prepared according to the literature methods.[8] Benzyl cyanide, PPN^+Cl^- (bis(triphenylphosphoranylidene)ammonium chloride), and Proton Sponge (PS, 1,8-bis(dimethylamino)naphthalene) were purchased from Aldrich and used as received. Sulfuric acid (99.999%) and 1.0 M HCl/Et_2O were purchased from Aldrich and stored under N_2 until use. The labeled $CH_3{}^{13}CN$ was prepared as reported previously.[9] Acetonitrile and methylene chloride were dried by distillation over P_2O_5 and freshly distilled from molecular sieves before use.

[⊗] Abstract published in *Advance ACS Abstracts,* June 15, 1996.

S0002-7863(96)00787-1 CCC: $12.00

Diethyl ether was dried over sodium benzophenone and freshly distilled before use. Heptane and hexane were purchased from Fisher and used as received. Oil dispersed NaH was obtained from Aldrich, washed with dry hexane under a nitrogen atmosphere, and then vacuum dried.

Physical Measurements. ^{1}H NMR spectra at 200.1 MHz and ^{11}B NMR at 64.2 MHz were obtained on a Bruker AF-200 spectrometer, equipped with the appropriate decoupling accessories. ^{1}H NMR spectra at 500.1 MHz, ^{11}B NMR spectra at 160.5 MHz, and ^{13}C NMR spectra at 125.7 MHz were obtained on a Bruker AM-500 spectrometer. All ^{11}B chemical shifts are referenced to external $BF_3{\cdot}O(C_2H_5)_2$ (0.0 ppm) with a negative sign indicating an upfield shift. All ^{1}H and ^{13}C chemical shifts were measured relative to internal residual protons or carbons in the lock solvents and are referenced to Me_4Si (0.0 ppm). Two-dimensional COSY ^{11}B−^{11}B NMR experiments were performed at 64.2 or 160.5 MHz using the procedures described previously.[10] Infrared spectra were obtained on a Perkin-Elmer 7770 Fourier transform spectrometer or a Perkin-Elmer 1430 spectrophotometer. Microanalysis was performed at Robertson Microlit, Madison, NJ. Melting points were obtained on a standard melting point apparatus and are uncorrected.

Synthesis of PPN$^+$-*arachno*-7-CH$_3$-5,7,14,12-C$_3$NB$_8$H$_{11}^-$ (PPN$^+$1$^-$). A 100-mL round-bottom flask fitted with a vacuum stopcock was charged with 0.46 g (3.76 mmol) of *nido*-5,6-$C_2B_8H_{12}$ and 0.17 g (7.08 mmol) of NaH. The flask was connected to the vacuum line and 50 mL of acetonitrile vacuum distilled into the flask at −196 °C. The mixture was then allowed to warm to room temperature. After the gas evolution ceased (∼40 min), the solution was filtered into another 100-mL flask under a N_2 atmosphere. The ^{11}B NMR spectrum taken after reflux for 10 days under a N_2 atmosphere showed complete disappearance of the *nido*-5,6-$C_2B_8H_{11}^-$. At this time, 2.16 g (3.76 mmol) of PPN$^+$Cl$^-$ was added to the flask and the mixture stirred at room temperature for 2 h. The acetonitrile was then vacuum evaporated and 20 mL of CH_2Cl_2 added. After filtration of the solution, ∼20 mL of diethyl ether and ∼5 mL of heptane were added and the solution filtered again. Slow evaporation of the remaining solvent afforded 1.73 g (2.46 mmol, 65.4% yield) of white, crystalline PPN$^+$-*arachno*-7-CH$_3$-5,7,14,12-C$_3$NB$_8$H$_{11}^-$ (PPN$^+$**1**$^-$). Anal. Calcd: C, 68.35%; H, 6.41%; N, 3.99%. Found: C, 67.68%; H, 6.11%; N, 4.01%. IR (KBr, cm^{-1}) 3360 (s), 3020 (m), 2935 (m), 2525 (vs), 2480 (vs), 1530 (m), 1480 (s), 1420 (m), 1360 (m), 1215 (m), 1160 (m), 1150 (m), 1090 (m), 1050 (w), 980 (m), 950 (m), 775 (w), 735 (w), 700 (w), 655 (w), 580 (w), 515 (w).

Acidification of *arachno*-7-CH$_3$-5,7,14,12-C$_3$NB$_8$H$_{11}^-$ (PPN$^+$1$^-$): Synthesis of *nido*-6-CH$_3$-5,6,9-C$_3$B$_7$H$_{10}$. In a 100-mL round-bottom flask, 1.93 g (2.75 mmol) of PPN$^+$-*arachno*-7-CH$_3$-5,7,14,12-C$_3$NB$_8$H$_{11}^-$ was dissolved in 20 mL of CH_2Cl_2. The solution was maintained at 0 °C, while 5 mL of H_2SO_4 was slowly added. The solution was then stirred for 30 min. The CH_2Cl_2 layer was removed and the H_2SO_4 layer extracted twice with CH_2Cl_2. Vacuum fractionation of the combined CH_2Cl_2 solutions through −45 and −196 °C traps afforded 0.11 g (0.80 mmol, 41.5% yield) of *nido*-6-CH$_3$-5,6,9-C$_3$B$_7$H$_{10}$ in the −45 °C trap, which was identified by comparison of its ^{11}B NMR and mass spectrum with literature values.[5]

Synthesis of PSH$^+$-*arachno*-7-CH$_3$-7,12-CNB$_{10}$H$_{13}^-$ (PSH$^+$2a$^-$). A 100-mL round-bottom flask fitted with a vacuum stopcock was charged with 0.59 g (4.82 mmol) of *nido*-$B_{10}H_{14}$ and 1.14 g (5.32 mmol) of Proton Sponge. The flask was connected to the vacuum line and 20 mL of acetonitrile was added by vacuum distillation. The flask was warmed to room temperature, which resulted in the formation of *nido*-$B_{10}H_{13}^-$, as evidenced by ^{11}B NMR.[11] The flask was fitted with a condenser and the reaction mixture refluxed under a N_2 atmosphere for 4 days. The acetonitrile was removed in vacuo to leave a red oil, which was then dissolved in CH_2Cl_2. Hexane was slowly added, causing separation of a red layer at the bottom with the product forming a suspension in the yellow CH_2Cl_2/hexane layer. Separation of the yellow layer and subsequent extraction of the red oil with additional CH_2Cl_2/hexane gave, after removal of the solvent, 0.98 g (2.59 mmol, 53.7% yield) of PSH$^+$-*arachno*-7-CH$_3$-7,12-CNB$_{10}$H$_{13}^-$ (PSH$^+$**2a**$^-$), as a yellow solid. Anal. Calcd: C, 50.90%; H, 9.34%; N, 11.13%; B, 28.63%. Found: C, 50.50%; H, 9.40%; N, 10.84%; B 28.42%. IR (KBr, cm^{-1}) 3310 (m), 3030 (w), 2950 (w), 2510 (vs), 2470 (vs), 1510 (w), 1460 (m), 1410 (w), 1380 (w), 1230 (w), 1195 (w), 1125 (w), 1040 (m), 1010 (w), 840 (w), 775 (m), 595 (w), 385 (w).

Synthesis of PSH$^+$-*arachno*-7-CH$_3$-7,12-^{13}CNB$_{10}$H$_{13}^-$ (PSH$^+$2a$^-$-^{13}C). In a similar manner as described above, 0.81 g (6.63 mmol) of *nido*-$B_{10}H_{14}$ and 1.46 g (6.81 mmol) of Proton Sponge were dissolved in 5 mL of $CH_3{}^{13}CN$. The reaction was refluxed for 2 days and the subsequent isolation afforded a crude yield of 1.85 g (4.89 mmol, 73.8% crude yield) of PSH$^+$-*arachno*-7-CH$_3$-7,12-^{13}CNB$_{10}$H$_{13}^-$ (PSH$^+$**2a**$^-$-^{13}C) as a yellow solid.

Synthesis of PSH$^+$-*arachno*-7-Bn-7,12-CNB$_{10}$H$_{13}^-$ (PSH$^+$2b$^-$). A 250-mL round-bottom flask fitted with a vacuum stopcock was charged with 2.00 g (16.37 mmol) of *nido*-$B_{10}H_{14}$ and 3.46 g (16.14 mmol) of Proton Sponge. This mixture was then dissolved in 20 mL of benzyl cyanide. The flask was fitted with a condenser and the reaction mixture heated at 80 °C under a N_2 atmosphere for 2 days. The remaining benzyl cyanide was removed in vacuo by heating at 100 °C for 3 h to leave a red oil, which was then dissolved in CH_2Cl_2. Fractional recrystallization by addition of hexane caused precipitation of an orange oily material. This material was redissolved in CH_2Cl_2 and isolated as a solid by addition of the CH_2Cl_2 solution to a large excess of heptane.

(1) (a) Hertler, W. R.; Klanberg, F.; Muetterties, E. L. *Inorg. Chem.* **1967**, *6*, 1696−1706. (b) Baše, K.; Plešek, J.; Heřmánek, S. *J. Chem. Soc., Chem. Commun.* **1975**, 934−935. (c) Plešek, J.; Heřmánek, S.; Huffman, J.; Ragatz, P.; Schaeffer, R. *J. Chem. Soc., Chem. Commun.* **1975**, 935−936. (d) Štíbr, B.; Baše, K.; Plešek, J.; Heřmánek, S.; Dolanský, J.; Janoušek, Z. *Pure Appl. Chem.* **1977**, *49*, 803−811. (e) Baše, K.; Štíbr, B.; Zakharova, I. A. *Synth. React. Inorg. Met.-Org. Chem.* **1980**, *10*, 509−514. (f) Bicerano, J.; Lipscomb, W. N. *Inorg. Chem.* **1980**, *19*, 1825−1827. (g) Dolanský, J.; Heřmánek, S.; Zahradník, R. *Collect. Czech. Chem. Commun.* **1981**, *46*, 2479−2493. (h) Baše, K.; Hanousek, F.; Plešek, J.; Štíbr, B. *J. Chem. Soc., Chem. Commun.* **1981**, 1162−1163. (i) Baše, K. *Collect. Czech. Chem. Commun.* **1983**, *48*, 2593−2603. (j) Todd, L. J.; Arafat, A.; Baer, J.; Huffman, J. C. *Mol. Struct. Energ., Adv. Boron Boranes* **1986**, *5*, 287−295. (k) Arafat, A.; Baer, J.; Huffman, J. C.; Todd, L. J. *Inorg. Chem.* **1986**, *25*, 3757−3761. (l) Boese, R.; Kröckert, B.; Paetzold, P. *Chem. Ber.* **1987**, *120*, 1913−1915. (m) Küpper, S.; Paetzold, P. *Chem. Ber.* **1989**, *122*, 479−480. (n) Štíbr, B.; Kennedy, J. D.; Jelínek, T. *J. Chem. Soc., Chem. Commun.* **1990**, 1309−1310. (o) Müller, J.; Paetzold, P.; Boese, R. *Heteroat. Chem.* **1990**, *1*, 461−465. (p) Müller, J.; Runsink, J.; Paetzold, P. *Angew. Chem., Int. Ed. Eng.* **1991**, *30*, 175. (q) Zahradník, R.; Balaji, V.; Michl, J. *J. Comput. Chem.* **1991**, *12*, 1147−1156. (r) Paetzold, P. *Pure Appl. Chem.* **1991**, *63*, 345−350. (s) Nöth, H.; Geisberger, G.; Linti, G.; Loderer, D.; Rattay, W.; Salzbrenner, E. *Pure Appl. Chem.* **1991**, *63*, 351−355. (t) Müller, J.; Paetzold, P.; Englert, U.; Runsink, J. *Chem. Ber.* **1992**, *125*, 97−102. (u) Meyer, F.; Müller, J.; Paetzold, P.; Boese, R. *Angew. Chem., Int. Ed. Engl.* **1992**, *31*, 1227−1229. (v) Hnyk, D.; Bühl, M.; Schleyer, P. v. R.; Volden, H. V.; Gundersen, S.; Müller, J.; Paetzold, P. *Inorg. Chem.* **1993,** *32*, 2442−2445. (w) Meyer, F.; Müller, J.; Schmidt, M. U.; Paetzold, P. *Inorg. Chem.* **1993,** *32*, 5053−5057. (x) Jelínek, T.; Kennedy, J. D.; Štíbr, B. *J. Chem. Soc., Chem. Commun.* **1993**, 1628−1629. (y) Paetzold, P.; Müller, J.; Meyer, F.; Hansen, H-P.; Schneider, L. *Pure Appl. Chem.* **1994**, *66*, 255−262. (z) Jelínek, T.; Kennedy, J. D.; Štíbr, B. *J. Chem. Soc., Chem. Commun.* **1994**, 677−678. (aa) Roth, M.; Paetzold, P. *Chem. Ber.* **1995**, *128*, 1221−1224. (bb) Lomme, P.; Meyer, F.; Englert, U.; Paetzold, P. *Chem. Ber.* **1995**, *128*, 1225−1229.

(2) (a) Kester, J. G.; Huffman, J. C.; Todd, L. J. *Inorg. Chem.* **1988**, *27*, 4528−4532. (b) Baše, K.; Bown, M.; Fontaine, X. L. R.; Greenwood, N. N.; Kennedy, J. D.; Štíbr, B.; Thornton-Pett, M. *J. Chem. Soc., Chem. Commun.* **1988**, 1240−1241. (c) Nestor, K.; Fontaine, X. L. R.; Kennedy, J. D.; Štíbr, B.; Baše, K.; Thornton-Pett, M. *Collect. Czech. Chem. Commun.* **1991**, *56*, 1607−1617.

(3) Plešek, J.; Štíbr, B.; Heřmánek, S. *Chem. Ind. (London)* **1974**, 662−663.

(4) Janoušek, Z.; Fusek, J.; Štíbr, B. *J. Chem. Soc., Dalton Trans*. **1992**, 2649−2650.

(5) Holub, J.; Jelinek, T.; Plešek, J.; Štíbr, B.; Heřmánek, S.; Kennedy, J. D. *J. Chem. Soc., Chem. Commun.* **1991**, 1389−1390.

(6) Kang, S. O.; Furst, G. T.; Sneddon, L. G. *Inorg. Chem.* **1989**, *28*, 2339−2347.

(7) Shriver, D. F.; Drezdzon, M. A. *Manipulation of Air Sensitive Compounds*, 2nd ed., Wiley: New York, 1986.

(8) Plešek, J.; Heřmánek, S. *Collect. Czech. Chem. Commun.* **1974**, *39*, 821−826.

(9) Plumb, C. A.; Sneddon, L. G. *Organometallics* **1992**, *11*, 1681−1685.

(10) Kang, S. O.; Carroll, P. J.; Sneddon, L. G. *Organometallics* **1988**, *7*, 772−776.

(11) Chambers, J. Q.; Norman, A. D.; Bickell, M. R.; Cadle, S. H. *J. Am. Chem. Soc.* **1968**, *90*, 6056−6062.

(12) *teXsan*: Crystal Structure Analysis Package, Molecular Structure Corporation, (1985 and 1992).

The solid was removed by filtration and dried under vacuum to yield 3.48 g (7.67 mmol, 46.9% yield) of PSH^+-*arachno*-7-Bn-7,12-$CNB_{10}H_{13}^-$ (PSH^+**2b**$^-$) as a yellow solid. Anal. Calcd: C, 58.25%; H, 8.66%; N, 9.26%. Found: C, 58.20%; H, 7.53%; N, 8.63%. IR (KBr, cm^{-1}) 3320 (w), 3060 (w), 3025 (w), 2960 (w), 2920 (w), 2510 (vs), 1605 (w), 1490 (m), 1455 (s), 1415 (m), 1385 (m), 1270 (m), 1225 (m), 1185 (m), 1160 (m), 1100 (w), 1080 (w), 1030 (m), 1005 (m), 835 (w), 770 (m), 705 (m), 610 (w), 490 (w), 420 (w).

Synthesis of *hypho*-12-CH_3-12,13-CNB_9H_{15} (3a). In a 100-mL round-bottom flask, 2.41 g (6.38 mmol) of PSH^+**2a**$^-$ was dissolved in 50 mL of CH_2Cl_2. The solution was maintained at 0 °C, while 10 mL of H_2SO_4 was slowly added. The solution was then stirred for 6 h. The CH_2Cl_2 layer was removed and the H_2SO_4 layer extracted twice with CH_2Cl_2. The combined CH_2Cl_2 solutions were vacuum evaporated at −30 °C. Then, 50 mL of hexane was added and the solution was filtered. The solution was concentrated in vacuo at −30 °C. The product was recrystallized from CH_2Cl_2 and hexane to yield 0.06 g (0.39 mmol, 6.1% yield) of *hypho*-12-CH_3-12,13-CNB_9H_{15} (**3a**) as a white solid. Mp 62−63 °C. Anal. Calcd: C, 15.65%; H, 11.82%; N, 9.13%; B, 63.40%. Found: C, 16.20%; H, 11.29%; N, 8.64%; B, 59.29%. IR (KBr, cm^{-1}) 3290 (s), 2955 (m), 2560 (s, br), 2190 (m), 1455 (m), 1390 (w), 1320 (w), 1265 (w), 1145 (w), 1095 (m), 1080 (m), 1010 (m), 890 (w), 835 (w), 815 (w), 740 (m), 710 (w), 670 (w), 625 (w), 595 (w), 525 (w). Exact mass calcd for $^{12}C_2{}^{11}B_9{}^{14}N^1H_{18}$ 155.2277, found 155.2272.

Synthesis of *hypho*-12-CH_3-12,13-$^{13}CNB_9H_{15}$ (3a-^{13}C). In a 100-mL round-bottom flask, 2.31 g (6.11 mmol) of PSH^+**2a**$^-$-^{13}C was dissolved in 50 mL of CH_2Cl_2. The solution was maintained at 0 °C, while 10 mL of H_2SO_4 was slowly added. The **3a**-^{13}C was then isolated as described above for the unlabeled compound to give a white solid in similar yield (∼0.05 g, 0.32 mmol, 5% yield).

Synthesis of *hypho*-12-Bn-12,13-CNB_9H_{15} (3b). In a 250-mL round-bottom flask, 50 mL of CH_2Cl_2 was added to 20 mL of H_2SO_4. The solution was maintained at 0 °C, while 9.60 g (21.16 mmol) of PSH^+**2b**$^-$ dissolved in 200 mL of CH_2Cl_2 was slowly added. The solution was then stirred for 5 h. The CH_2Cl_2 layer was removed and the H_2SO_4 layer extracted twice with CH_2Cl_2. The combined CH_2Cl_2 solutions were vacuum evaporated at −30 °C. Then, 50 mL of hexane was added and the solution was filtered. The solution was concentrated by vacuum evaporation at −30 °C. The product was recrystallized from CH_2Cl_2 and hexane to yield 0.32 g (1.39 mmol, 6.6% yield) of *hypho*-12-Bn-12,13-CNB_9H_{15} (**3b**) as a white solid. Mp 136−38 °C, Anal. Calcd: C, 41.86%; H, 9.66%; N, 6.10%. Found: C, 42.01%; H, 9.56%; N, 5.76%. IR (KBr, cm^{-1}) 3290 (m), 3070 (w), 3040 (w), 2930 (w), 2560 (vs), 1605 (w), 1560 (w), 1495 (w), 1455 (m), 1390 (w), 1265 (w), 1190 (m), 1090 (m), 1030 (w), 1005 (m), 820 (w), 750 (m), 705 (m), 610 (w). Exact mass calcd for $^{12}C_8{}^{11}B_9{}^{14}N^1H_{22}$ 231.2590, found 231.2594.

Synthesis of *hypho*-12-CH_3-12,13-$CNB_9H_{14}^-$ (PSH^+3a**$^-$).** Samples for spectroscopic analysis were synthesized by addition of an excess of Proton Sponge in CH_2Cl_2 to a solution of ∼0.05 g of **3a** in CH_2Cl_2. After the solution was stirred for 5 min, the product, PSH^+**3a**$^-$, was precipitated by addition of hexane to a CH_2Cl_2 solution and the solvent was decanted. Washing with additional hexane and drying under vacuum for 1 h afforded PSH^+-*hypho*-12-CH_3-12,13-$CNB_9H_{14}^-$ (PSH^+**3a**$^-$) as a crude, yellow solid in estimated quantitative yield. Samples could be stored at −78 °C but decomposed to PSH^+**4a**$^-$ after several hours at room temperature. IR (KBr, cm^{-1}) 3290 (m), 3060 (w), 2940 (m), 2865 (m), 2830 (w), 2790 (w), 2500 (vs), 1580 (w), 1465 (m), 1455 (m), 1420 (m), 1390 (m), 1265 (w), 1225 (m), 1190 (m), 1165 (w), 1140 (w), 1100 (s), 1030 (s), 940 (w), 835 (w), 770 (s), 610 (w).

Synthesis of *hypho*-12-CH_3-12,11-$CNB_9H_{14}^-$ (PSH^+4a**$^-$).** In a 100-mL round-bottom flask, 0.08 g (0.52 mmol) of **3a** was dissolved in 20 mL of CH_2Cl_2. To this was added a solution of 0.12 g (0.56 mmol) of Proton Sponge dissolved in 2 mL of CH_2Cl_2. Then, the solution was stirred overnight at room temperature. The anion was precipitated by addition of hexane to the CH_2Cl_2 solution and the solvent was decanted. Washing with additional hexane and drying under vacuum afforded 0.17 g (0.46 mmol, 88.5% yield) of PSH^+-*hypho*-12-CH_3-12,11-$CNB_9H_{14}^-$ (PSH^+**4a**$^-$) as a yellow solid. IR (KBr, cm^{-1}) 3290 (s), 2960 (w), 2940 (m), 2910 (w), 2880 (w), 2860 (w), 2530 (s), 2490 (vs), 2430 (s), 2350 (w), 1465 (m), 1430 (m), 1415 (m), 1395 (m), 1360 (m), 1310 (m), 1265 (w), 1230 (w), 1190 (m), 1165 (m), 1150 (m), 1100 (s), 1010 (m), 970 (w), 930 (w), 840 (m), 820 (w), 775 (s), 725 (w), 595 (w), 485 (w). Anal. Calcd: C, 52.25%; H, 9.87%; N, 11.43%; B, 26.45%. Found: C, 51.88%; H, 9.68%; N, 10.89%; B, 26.20%.

Synthesis of *hypho*-12-CH_3-12,13-$^{13}CNB_9H_{14}^-$ (PSH^+3a**$^-$-^{13}C) and *hypho*-12-CH_3-12,11-$^{13}CNB_9H_{14}^-$ (PSH^+**4a**$^-$-^{13}C).** To a sample of **3a**-^{13}C (∼0.05 g, 0.32 mmol) in CH_2Cl_2 was added an excess of Proton Sponge in CH_2Cl_2. After 5 min, an NMR sample was removed and used to obtain the ^{11}B NMR spectra of PSH^+**3a**$^-$-^{13}C. The remainder of the solution was stirred overnight. The anion was isolated as described above for the unlabeled compound to give PSH^+**4a**$^-$-^{13}C as a yellow solid (∼0.1 g, 0.27 mmol, 80% yield).

Synthesis of *hypho*-12-Bn-12,13-$CNB_9H_{14}^-$ (PSH^+3b**$^-$).** Samples for spectroscopic analysis were synthesized by addition of an excess of Proton Sponge in CH_2Cl_2 to a solution of ∼0.05 g of **3b** in CH_2Cl_2. After the solution was stirred for 5 min, PSH^+**3b**$^-$ was isolated as described above for PSH^+**3a**$^-$ to give PSH^+-*hypho*-12-Bn-12,13-$CNB_9H_{14}^-$ (PSH^+**3b**$^-$) as a crude, yellow solid in estimated quantitative yield. Samples could be stored at −78 °C, but decomposed to PSH^+**4b**$^-$ after several hours at room temperature. IR (KBr, cm^{-1}) 3320 (m), 3060 (w), 3030 (w), 2960 (w), 2930 (w), 2860 (w), 2500 (vs), 1605 (w), 1465 (m), 1455 (m), 1415 (w), 1385 (w), 1270 (w), 1225 (m), 1185 (m), 1160 (m), 1080 (s), 1030 (s), 1005 (s), 835 (w), 770 (s), 705 (w), 605 (w).

Synthesis of *hypho*-12-Bn-12,11-$CNB_9H_{14}^-$ (PSH^+4b**$^-$).** In a 100-mL round-bottom flask, 0.11 g (0.48 mmol) of **3b** was dissolved in 10 mL of CH_2Cl_2. To this was added a solution of 0.13 g (0.61 mmol) of Proton Sponge dissolved in 10 mL of CH_2Cl_2. After the solution was stirred overnight, the resulting anion was isolated as described above for PSH^+**4a**$^-$ to yield 0.13 g (0.29 mmol, 60.4% yield) of PSH^+-*hypho*-12-Bn-12,11-$CNB_9H_{14}^-$ (PSH^+**4b**$^-$). IR (KBr, cm^{-1}) 3280 (m), 3060 (w), 3020 (w), 2960 (w), 2920 (w), 2850 (w), 2490 (s), 1605 (w), 1465 (m), 1455 (m), 1415 (s), 1395 (s), 1310 (s), 1225 (m), 1185 (m), 1165 (m), 1115 (m), 1090 (m), 1065 (m), 1020 (m), 930 (m), 835 (m), 770 (s), 705 (m), 625 (w), 485 (w), 420 (w), 385 (w). Anal. Calcd: C, 59.53%; H, 9.08%; N, 9.47%. Found: C, 56.35%; H, 8.66%; N, 8.82%.

Acidification of *hypho*-12-R-12,13-$CNB_9H_{14}^-$ (PSH^+3a**$^-$ and PSH^+**3b**$^-$).** To an NMR sample of either PSH^+**3a**$^-$ or PSH^+**3b**$^-$ in CH_2Cl_2 was added an excess of 1.0 M HCl/Et_2O. This resulted in the immediate regeneration of the original neutral molecules, **3a** or **3b**, respectively, as observed by ^{11}B NMR.

Synthesis of *hypho*-8-CH_3-8,13-CNB_8H_{14} (5a). In a 100-mL round-bottom flask, 0.09 g (0.24 mmol) of PSH^+**4a**$^-$ was dissolved in 20 mL of CH_2Cl_2. The solution was maintained at 0 °C, 2 mL of H_2SO_4 was added dropwise, and the solution was stirred for several hours. The CH_2Cl_2 layer was removed and the H_2SO_4 layer extracted twice with CH_2Cl_2 and the combined CH_2Cl_2 solutions then concentrated by vacuum evaporation at −30 °C. Then, 20 mL of hexane was added and the solution was dried over $MgSO_4$ and filtered. The resulting solution was fractionated overnight through −50 and −196 °C traps. The −50 °C trap contained 0.02 g (0.14 mmol, 58.3% yield) of *hypho*-8-CH_3-8,13-CNB_8H_{14} (**5a**) as a colorless liquid. IR (CCl_4 sol, NaCl plates, cm^{-1}) 3330 (s), 2960 (m), 2930 (w), 2900 (w), 2870 (w), 2560 (s, br), 1450 (m), 1380 (w), 1350 (m), 1315 (w), 1260 (w), 1200 (w), 1150 (m), 1105 (m), 1070 (w), 1045 (w), 995 (w), 980 (w), 935 (m), 910 (w), 890 (w). Exact mass calcd for $^{12}C_2{}^{11}B_8{}^{14}N^1H_{17}$ 143.2105, found 143.2108.

Synthesis of *hypho*-8-CH_3-8,13-$^{13}CNB_8H_{14}$ (5a-^{13}C). A sample of PSH^+**4a**$^-$-^{13}C (∼0.1 g, 0.27 mmol) was dissolved in CH_2Cl_2 and reacted with H_2SO_4 for 2 h in a similar manner as described above for the unlabeled compound. The CH_2Cl_2 layer was removed and concentrated by vacuum evaporation at −30 °C. Hexane was added, the solution was filtered, and the solvent was removed at −30 °C. The resulting oil was dissolved in CD_2Cl_2 to obtain the ^{11}B NMR spectrum of **5a**-^{13}C.

Synthesis of *hypho*-8-Bn-8,13-CNB_8H_{14} (5b). In a 100-mL round-bottom flask, 0.13 g (0.29 mmol) of PSH^+**4b**$^-$ was dissolved in 20 mL of CH_2Cl_2. The solution was maintained at 0 °C, 2 mL of H_2SO_4 was added dropwise, and the solution was stirred for several hours. The CH_2Cl_2 layer was removed, the H_2SO_4 layer was extracted twice

with CH_2Cl_2, and the combined CH_2Cl_2 solutions were concentrated by vacuum evaporation at −30 °C. Then, 20 mL of hexane was added and the solution was dried over $MgSO_4$ and filtered. The solvent was vacuum evaporated at −30 °C and the solid was recrystallized from hexane at −78 °C and dried in vacuo to yield 0.04 g (0.18 mmol, 62.0% yield) of *hypho*-8-Bn-8,13-CNB_8H_{14} (**5b**) as a white solid. Mp 102−104 °C. IR (KBr, cm^{-1}) 3300 (s), 3030 (w), 2920 (m), 2880 (w), 2850 (w), 2540 (vs), 2500 (s), 2480 (s), 1490 (m), 1450 (m), 1355 (m), 1280 (m), 1125 (m), 1080 (m), 1065 (m), 1050 (m), 1030 (w), 1000 (w), 930 (m), 885 (w), 830 (w), 750 (m), 705 (m), 625 (w), 605 (w), 545 (w), 500 (w). Exact mass calcd for $^{12}C_8{}^{11}B_8{}^{14}N^1H_{21}$ 219.2419, found 219.2426.

Synthesis of *hypho*-8-R-8,13-$CNB_8H_{13}^-$ (PSH^+5a$^-$, PSH^+5b$^-$). Samples for spectroscopic analysis were prepared in good yield by addition of an excess of Proton Sponge to a solution of **5a** or **5b** in CH_2Cl_2. The resulting anion was precipitated by addition of hexane and the solvent decanted. Washing with additional hexane and drying under vacuum yielded a crude sample of either *hypho*-8-CH_3-8,13-$CNB_8H_{13}^-$ (PSH^+**5a**$^-$) or *hypho*-8-Bn-8,13-$CNB_8H_{13}^-$ (PSH^+**5b**$^-$), which were found to be too unstable for complete characterization.

Synthesis of *hypho*-8-CH_3-8,13-$^{13}CNB_8H_{13}^-$ (PSH^+5a$^-$-^{13}C). To an NMR sample of **5a**-^{13}C in CD_2Cl_2 was added excess Proton Sponge. The formation of PSH^+**5a**$^-$-^{13}C was observed by ^{11}B NMR.

Acidification of *hypho*-8-CH_3-8,13-$CNB_8H_{13}^-$ (PSH^+5a$^-$). To an NMR sample of PSH^+**5a**$^-$ in CH_2Cl_2 was added an excess of 1.0 M HCl/Et_2O. This resulted in the immediate regeneration of the original neutral molecule **5a**, as observed by ^{11}B NMR.

Crystallographic Data. Single crystals of PPN^+-*arachno*-7-CH_3-5,7,14,12-$C_3NB_8H_{11}^-$ (PPN^+**1**$^-$) were grown by slow evaporation of CH_2Cl_2/Et_2O/heptane solutions under argon. The crystal of PPN^+**1**$^-$ was mounted inside a capillary tube which was then sealed with glue and mounted on the diffractometer. Single crystals of PSH^+-*arachno*-7-CH_3-7,12-$CNB_{10}H_{13}^-$ (PSH^+**2a**$^-$), *hypho*-12-Bn-12,13-CNB_9H_{15} (**3b**), and PSH^+*hypho*-12-CH_3-12,11-$CNB_9H_{14}^-$ (PSH^+**4a**$^-$) were grown by slow evaporation of CH_2Cl_2/hexane solutions. The cell constants for all compounds were determined from a least-squares fit of the setting angles for 25 accurately centered reflections.

Collection and Refinement of the Data. For PPN^+**1**$^-$ and PSH^+**2a**$^-$, X-ray intensity data were collected on an Enraf-Nonius CAD4 diffractometer employing graphite-monochromated Cu Kα radiation and using the ω-2θ scan technique. For PSH^+**4a**$^-$, the data were collected on a MSC/AFC7R diffractometer employing graphite-monochromated Cu Kα radiation and using the $\omega-2\theta$ scan technique. For **3b**, the data were collected on an MSC/R-AXIS IIc area detector employing graphite-monochromated Mo Kα radiation with 6° oscillations, exposures of 5 min per frame, a crystal to detector distance of 82 mm, and a temperature of 235 K. For PPN^+**1**$^-$, PSH^+**2a**$^-$, and PSH^+**4a**$^-$, three standard reflections measured every 3500 s of X-ray exposure, over the course of data collection, showed no intensity decay for PPN^+**1**$^-$, and 0.7% and 7.83% decay for PSH^+**2a**$^-$ and PSH^+**4a**$^-$, respectively. A linear decay correction was applied to PSH^+**2a**$^-$ and PSH^+**4a**$^-$. The intensity data for all structures were corrected for Lorentz and polarization effects, but not for absorption.

Solution and Refinement of the Structures. The calculations for PPN^+**1**$^-$ and PSH^+**2a**$^-$ were performed on a DEC MicroVAX 3100 computer using the Enraf-Nonius Molen structure package. The calculations for **3b** and PSH^+**4a**$^-$ were performed on a Silicon Graphics Indigo R4000 computer using the Molecular Structure Corporation teXsan[12] package. The structures were solved by direct methods (MULTAN11/82, SIR88 or SIR92). Refinement was by full-matrix least-squares techniques based on F to minimize the quantity $\sum w(|F_o| - |F_c|)^2$ with $w = 1/\sigma^2(F)$. For PPN^+**1**$^-$, PSH^+**2a**$^-$, and **3b**, non-hydrogen atoms were refined anisotropically and hydrogens were refined isotropically. For PSH^+**4a**$^-$, non-hydrogen atoms were refined anisotropically and hydrogens were refined isotropically, except for the cage-methyl hydrogens and the hydrogen on N2 which were included as constant contributions to the structure factors and were not refined.

Crystal and refinement data are given in Table 2. Refined positional parameters are given in tables in the supporting information. Selected intramolecular bond distances are presented in Tables 3−6.

Computational Methods. The combined ab initio/IGLO/NMR method, using the GAUSSIAN90[13] and GAUSSIAN92[14] programs, was used as described previously.[15] The geometries were fully optimized at the HF/6-31G* level within the specified symmetry constraints (using the standard basis sets included) on a Silicon Graphics International IRIS 4D/440VGX computer. Selected calculated intramolecular bond distances are compared to the crystallographically determined distances in tables in the supporting information. A vibrational frequency analysis was carried out on each optimized geometry at the HF/3-21G level and a true minimum was found for each structure (i.e. possessing no imaginary frequencies). The NMR chemical shifts were calculated using the IGLO program employing the following basis sets. Basis DZ: C, B, N 7s3p contracted to [4111, 21]; H 3s contracted to [21].

Results and Discussion

The isoelectronic, 10-vertex *nido*-5,6-$C_2B_8H_{11}^-$ and *nido*-$B_{10}H_{13}^-$ anions were both found to readily react with nitriles to produce new azacarborane products in good yields (eqs 3 and 4).

$$\textit{nido}\text{-}5,6\text{-}C_2B_8H_{11}^- + CH_3CN \rightarrow \textit{arachno}\text{-}7\text{-}CH_3\text{-}5,7,14,12\text{-}C_3NB_8H_{11}^- \quad (\mathbf{1}^-) \qquad (3)$$

$$\textit{nido}\text{-}B_{10}H_{13}^- + RCN \rightarrow \textit{arachno}\text{-}7\text{-}R\text{-}7,12\text{-}CNB_{10}H_{13}^- \quad (R = CH_3,\ \mathbf{2a}^-;\ \mathbf{2a}^-\text{-}^{13}C) \quad (R = Bn,\ \mathbf{2b}^-) \qquad (4)$$

The products were isolated as air-stable, crystalline PPN^+ (**1**$^-$) or Proton Sponge H^+ salts (**2a**$^-$ and **2b**$^-$). Single-crystal structural determinations of PPN^+**1**$^-$ and PSH^+**2a**$^-$, shown in the ORTEP drawings in Figures 1 and 2, confirm insertion of both the nitrile carbon and nitrogen into the borane cluster framework to produce isoelectronic azatricarbaborane (**1**$^-$) and azamonocarbaborane (**2a**$^-$) anions. In both anions, the imine group bridges the B2 and B11 atoms and lies in a molecular mirror plane. Accordingly, both cages have two puckered six-membered open faces, containing the CN unit and four other cage atoms. In **1**$^-$, each face contains one of the original cage carbon atoms, at C5 or C14, whereas in **2**$^-$, each face contains one bridge hydrogen at the B1−B5 and B8−B14 edges. The C7−N12 bond distances in **1**$^-$ (1.310(3) Å) and **2a**$^-$ (1.307(3) Å) are consistent with reduction of the acetonitrile carbon−nitrogen triple bond and are similar to that found previously[6] in *hypho*-5-CH_3-5,11,7,14-$CNS_2B_7H_9$, (C5−N11, 1.298(5) Å).

The observed basket structures of **1**$^-$ and **2**$^-$ can be viewed in at least two ways. If the nitrile-derived carbon and nitrogen are considered to be part of the cluster framework, then each cluster would contain 30 skeletal electrons and be a 12-vertex arachno system ($n + 3$ skeletal electron pairs). On the basis of

(13) Frisch, M. J.; Head-Gordon, M.; Trucks, G. W.; Foresman, J. B.; Schlegel, H. B.; Raghavachari, K.; Robb, M.; Binkley, J. S.; Gonzalez, C.; Defrees, D. J.; Fox, D. J.; Whiteside, R. A.; Seeger, R.; Melius, C. F.; Baker, J.; Martin, R. L.; Kahn, L. R.; Stewart, J. J. P.; Topiol, S.; Pople, J. A. *Gaussian 90*, *Revision H*, Gaussian, Inc.: Pittsburgh, PA, 1990.

(14) Frisch, M. J.; Trucks, G. W.; Schlegel, H. B.; Gill, P. M. W.; Johnson, B. G.; Wong, M. W.; Foresman, J. B.; Robb, M. A.; Head-Gordon, M.; Replogle, E. S.; Gomperts, R.; Andres, J. L.; Raghavachari, K.; Binkley, J. S.; Gonzalez, C.; Martin, R. L.; Fox, D. J.; Defrees, D. J.; Baker, J.; Stewart, J. J. P.; Pople, J. A. *Gaussian 92/DFT*, *Revision F.2*; Gaussian, Inc.: Pittsburgh, PA, 1993.

(15) Keller, W.; Barnum, B. A.; Bausch, J. W.; Sneddon, L. G. *Inorg. Chem.* **1993**, *32*, 5058−5066.

Table 1. NMR Data

compounds	nucleus	δ (multiplicity, assignment, J (Hz))
arachno-7-CH_3-5,7,14,12-$C_3NB_8H_{11}$ (PPN^+**1**$^-$)	$^{11}B^{a,b}$	5.6 (d, B1,8, J_{BH} 132), 2.3 (d, B10, J_{BH} 154), −8.3 (d, B3, J_{BH} 132), −20.9 (d, B11, J_{BH} 114), −23.3 (d, B2, J_{BH} ∼160), −23.9 (d, B4,9, J_{BH} 134)
	^{11}B (calc)^c	4.6 (B1,8), 4.9 (B10), −5.9 (B3), −24.5 (B11), −27.7 (B2), −25.8 (B4,9)
	$^{11}B-^{11}B^{b,d}$	observed crosspeaks: B1,8−B2, B1,8−B3, B2−B3, B3−B4,9, B4,9−B10
	$^1H\{^{11}B\}^{b,e,f}$	6.46 (br, NH), 3.06 (1, BH), 2.50 (2, BH), 2.43 (s, CH_3), 1.87 (1, BH), 1.55 (s, 2, CH, 1, BH), 1.40 (1, BH), 1.20 (2, BH)
	$^{13}C^{b,f,g}$	210.5 (br, C7), 40.8 (d, br, C5,14, J_{CH} 151), 30.6 (q, C7a, J_{CH} 132)
arachno-7-CH_3-7,12-$CNB_{10}H_{13}^-$ (PSH^+**2a**$^-$)	$^{11}B^{a,b}$	−7.5 (d, B10, J_{BH} 142), −8.4 (d, B11, J_{BH} 161), −9.3 (d, B3, J_{BH} 130), −11.6 (d, B1,8, J_{BH} 135), −15.9 (d, B5,14, J_{BH} ∼175), −17.1 (d, B2, J_{BH} 125), −24.0 (d, B4,9, J_{BH} 134)
	^{11}B (calc)^c	−3.4 (B10), −12.4 (B11), −4.8 (B3), −13.9 (B1,8), −18.5 (B5,14), −22.5 (B2), −27.6 (B4,9)
	$^{11}B-^{11}B^{b,d}$	observed crosspeaks: B1,8−B2, B1,8−B4,9, B2−B3[h], B3−B4,9, B4,9−B5,14, B4,9−B10[h], B5,14−B10[h], B5,14−B11[h]
	$^1H\{^{11}B\}^{f,i,j}$	8.33 (br, NH), 2.91 (1, BH), 2.27 (s, CH_3), 2.02 (1, BH), 1.87 (1, BH), 1.27 (5, BH), 0.86 (2, BH), −8.08 (2, BHB)
	$^{13}C^{f,g,i}$	197.8 (br, C7), 30.6 (q, C7a, J_{CH} 129)
arachno-7-CH_3-7,12-$^{13}CNB_{10}H_{13}^-$ (PSH^+**2a**$^-$-^{13}C)	$^{11}B\{^1H\}^{a,b}$	−7.5 (s, B10), −8.5 (s, B3), −9.3 (s, B11), −11.6 (s, B1,8), −15.9 (s, B5,14), −17.2 (d, B2, $J_{^{11}B^{13}C}$ 57), −24.0 (s, B4,9)
	$^1H\{^{11}B\}^{b,f,j,k}$	2.49 (d, CH_3, $J_{H^{13}C}$ 5), 2.47 (1, BH), 2.26 (1, BH), 2.11 (1, BH), 1.53 (5, BH), 1.12 (2, BH), −7.74 (2, BHB)
	$^{13}C\{^1H\}^{b,f,g,l}$	197.3 (q, ^{13}C7, $J_{^{13}C^{11}B}$ 60)
arachno-7-Bn-7,12-$CNB_{10}H_{13}^-$ (PSH^+**2b**$^-$)	$^{11}B^{a,i}$	−7.0 (d, B10, J_{BH} ∼145), −8.0 (d, B3, J_{BH} obscured), −8.4 (d, B11, J_{BH} ∼120), −10.9 (d, B1,8, J_{BH} 124), −15.2 (d, B5,14, J_{BH} 122), −15.6 (d, B2, J_{BH} ∼100), −23.0 (d, B4,9, J_{BH} 135)
	$^1H\{^{11}B\}^{b,f,j,k}$	7.27 (m, br, C_6H_5), 4.24 (s, CH_2), 2.60 (1, BH), 2.33 (1, BH), 2.12 (1, BH), 1.56 (2, BH), 1.50 (2, BH), 1.37 (1, BH), 1.14 (2, BH), −7.76 (2, BHB)
hypho-12-CH_3-12,13-CNB_9H_{15} (**3a**)	$^{11}B^{a,m}$	15.9 (d, B4, J_{BH} 148), 3.8 (d, B11, J_{BH} 128), −7.1 (d, B2 or B8, J_{BH} 173), −8.4 (d, B2 or B8, J_{BH} 172), −19.6 (d, B1, B9, J_{BH} 146), −37.1 (d of d, B5 or B10, J_{BH} 190, $J_{B\mu H}$ 30), −38.5 (d of d, B5 or B10, J_{BH} 177, $J_{B\mu H}$ 35), −52.7 (d, B3, J_{BH} 150)
	^{11}B (calc)^c	17.8 (B4), 3.5 (B11), −7.6 (B2), −8.0 (B8), −13.9 (B1), −14.1 (B9), −36.6 (B5), −37.0 (B10), −57.6 (B3)
	$^{11}B-^{11}B^{d,m}$	observed crosspeaks: B1(B9)−B3, B1(B9)−B4, B1(B9)−B5(B10), B1(B9)−B10(B5), B1(B9)−B2(B8), B1(B9)−B8(B2), B2(B8)−B3, B8(B2)−B3, B3−B4, B4−B5(B10), B4−B10(B5)
	$^1H\{^{11}B\}^{f,j,m}$	4.39 (1, BH), 2.69 (1, BH), 2.58 (1, BH), 2.47 (1, BH), 2.38 (2, BH), 1.37 (2, BH), 1.01 (1, NH), 0.56 (br, 1, CH), 0.41 (1, BH), 0.15 (d, CH_3, J_{HH} 7), −1.04 (1, BHB), −1.53 (1, BHB), −1.61 (1, BHB), −1.68 (1, BHB)
	$^{13}C^{b,f,g}$	33.70 (br, C12), 20.4 (q, C12a, J_{CH} 127)
hypho-12-CH_3-12,13-$^{13}CNB_9H_{15}$ (**3a**-^{13}C)	$^{11}B\{^1H\}^{a,m}$	16.1 (s, B4), 4.1 (d, B11, $J_{^{11}B^{13}C}$ 53), −7.0 (s, B2 or B8), −8.3 (s, B2 or B8), −19.5 (s, B1,9), −36.9 (s, B5 or B10), −38.4 (s, B5 or B10), −52.6 (s, B3)
	$^1H\{^{11}B\}^{f,j,k,m,n}$	4.38 (1, BH), 2.69 (1, BH), 2.56 (1, BH), 2.47 (1, BH), 2.38 (2, BH), 1.36 (2, BH), 0.80 (br, 1, CH), 0.15 (d of d, CH_3, J_{HH} 7, $J_{H^{13}C}$ 3), −1.05 (1, BHB), −1.55 (1, BHB), −1.62 (1, BHB), −1.70 (1, BHB)
	$^{13}C\{^1H\}^{f,g,l,m}$	32.45 (d, ^{13}C12, $J_{^{13}C^{11}B}$ 60)
hypho-12-Bn-12,13-CNB_9H_{15} (**3b**)	$^{11}B^{a,b}$	15.5 (d, B4, J_{BH} 142), 3.9 (d, B11, J_{BH} 119), −6.6 (d, B2 or B8, J_{BH} 169), −8.1 (d, B2 or B8, J_{BH} 151), −19.5 (d, B1,9, J_{BH} 141), −37.6 (d of d, B5 or B10, J_{BH} ∼145, $J_{B\mu H}$ ∼40), −38.3 (d of d, B5 or B10, J_{BH} ∼125, $J_{B\mu H}$ ∼40), −52.9 (d, B3, J_{BH} 149)
	$^1H\{^{11}B\}^{b,f,j}$	7.23 (m, br, C_6H_5), 3.9 (br, NH), 3.71 (1, BH), 3.03 (1, BH), 2.93 (d, CH, J_{HH} 13), 2.69 (2, BH), 2.39 (t, CH, J_{CH} 12), 2.08 (s, CH), 1.97 (2, BH), 0.92 (2, BH), −0.28 (1, BH), −0.64 (1, BHB), −1.22 (2, BHB), −1.33 (1, BHB)
hypho-12-CH_3-12,13-$CNB_9H_{14}^-$ (PSH^+**3a**$^-$)	$^{11}B^{a,b}$	−2.5 (d, 1, J_{BH} 126), −16.9 (d, 1, J_{BH} 132), −19.2 (d, B11, J_{BH} 134), −21.0 (br, 1), −31.7 (d, 1, J_{BH} ∼135), −32.5 (d, 2, J_{BH} ∼137), −47.3 (br, 2)
	^{11}B (calc)^c	from structure in Figure 13a: 0.8 (B4), −10.4 (B5), −16.1 (B8), −19.9 (B2), −20.7 (B11), −27.5 (B3), −43.6 (B9), −48.9 (B1), −49.5 (B10) from structure in Figure 13b: 16.3 (B4), −11.5 (B11), −12.3 (B2), −18.4 (B8), −26.9 (B9), −28.7 (B5), −29.4 (B1), −36.9 (B10), −56.3 (B3)
	$^1H\{^{11}B\}^{b,f,j,n}$	2.71 (1, BH), 2.16 (1, NH), 1.97 (1, BH), 1.79 (1, BH), 1.45 (1, CH), 0.91 (d, CH_3, J_{HH} 7), 0.67 (2, BH), 0.62 (1, BH), −0.21 (1, BH), −0.37 (1, BH), −0.57 (1, BHB), −1.87 (1, BHB), −2.12 (1, BHB)
hypho-12-CH_3-12,13-$CNB_9H_{14}^-$ (PSH^+**3a**$^-$^{13}C)	$^{11}B\{^1H\}^{a,b}$	−2.3 (s, 1), −16.9 (s, 1), −19.0 (d, B11, $J_{^{11}B^{13}C}$ 106), −20.8 (s, 1), −32.3 (s, 3), −47.1 (br, 2)

Table 1 (Continued)

compounds	nucleus	δ (multiplicity, assignment, J (Hz))
hypho-12-Bn-12,13-$CNB_9H_{14}^-$ (PSH^+**3b**$^-$)	$^{11}B^{a,b}$	−2.0 (d, 1, J_{BH} 138), −16.9 (d, 1, J_{BH} 130), −19.0 (d, 1, J_{BH} 134), −21.5 (br, 1), −30.1 (d, 1, J_{BH} 119), −33.1 (d, 1, J_{BH} 138), −33.9 (d, 1, J_{BH} 131), −46.4 (br, 1), −46.8 (br, 1)
	$^1H\{^{11}B\}^{b,f,j,n}$	7.63 (m, br, C_6H_5), 2.74 (1, BH), 2.71 (d, CH, J_{HH} 14), 2.24 (t, CH, J_{HH} 14), 2.04 (1, NH), 1.79 (1, BH), 1.52 (2, CH, BH), 0.80 (1, BH), 0.61 (1, BH), 0.55 (1, BH), −0.29 (2, BH), −0.40 (1, BHB), −1.97 (2, BHB)
hypho-12-CH_3-12,11-$CNB_9H_{14}^-$ (PSH^+**4a**$^-$)	$^{11}B^{a,i}$	13.0 (d, B3, J_{BH} 131), 7.9 (d, B5, J_{BH} 143), 2.4 (d, B7, J_{BH} 121), −10.3 (d, B10, J_{BH} 144), −18.9 (t, B8, J_{BH} 108), −21.6 (d, B2, J_{BH} 116), −32.8 (d, B9, J_{BH} 130), −35.8 (d, B4, J_{BH} 129), −43.5 (d, B1, J_{BH} 128)
	^{11}B (calc)^c	16.2 (B3), 6.5 (B5), 3.5 (B7), −11.5 (B10), −12.0 (B8), −18.9 (B2), −31.2 (B9), −36.4 (B4), −47.7 (B1)
	$^{11}B-^{11}B^{d,i}$	observed crosspeaks: B1−B2, B1−B3, B1−B4, B1−B5, B1−B7, B2−B3, B2−B8, B3−B4, B3−B8, B3−B9, B4−B5, B4−B9, B4−B10, B8−B9
	$^1H\{^{11}B\}^{b,f,j}$	3.76 (1, BH), 3.44 (1, BH), 2.57 (1, BH), 2.49 (1, NH), 2.19 (1, BH), 1.38 (1, BH), 1.34 (1, CH), 1.10 (1, BH), 1.09 (d, CH_3, J_{HH} 7), 0.72 (1, BH), 0.17 (2, BH), −1.12 (1, BH), −2.51 (1, BHB), −2.59 (1, BHB)
	$^{13}C\{^1H\}^{f,g,i}$	46.7 (s, C12), 24.8 (s, CH_3)
hypho-12-CH_3-12,11-$^{13}CNB_9H_{14}^-$ (PSH^+**4a**$^{-13}$C)	$^{11}B\{^1H\}^{a,i}$	13.0 (s, B3), 7.9 (s, B5), 2.4 (br, B7, $J_{^{11}B^{13}C}$ obscured), −10.3 (s, B10), −18.9 (s, B8), −21.6 (d, B2), −32.8 (s, B9), −35.8 (s, B4), −43.5 (s, B1)
	$^1H\{^{11}B\}^{b,f,j}$	3.75 (1, BH), 3.43 (1, BH), 2.57 (1, BH), 2.47 (1, NH), 2.19 (1, BH), 1.38 (1, BH), 1.26 (br, CH), 1.14 (1, BH), 1.09 (d of d, CH_3, J_{HH} 7, $J_{H^{13}C}$ 3), 0.72 (1, BH), 0.17 (2, BH), −1.11 (1, BH), −2.51 (1, BHB), −2.60 (1, BHB)
	$^{13}C\{^1H\}^{f,g,i,l}$	45.5 (d, ^{13}C12, $J_{^{13}C^{11}B}$ 59)
hypho-12-Bn-12,11-$CNB_9H_{14}^-$ (PSH^+**4b**$^-$)	$^{11}B^{a,i}$	12.9 (d, B3, J_{BH} 121), 8.0 (d, B5, J_{BH} 139), 1.3 (d, B7, J_{BH} 123), −10.3 (d, B10, J_{BH} 126), −19.0 (t, B8, J_{BH} 94), −21.8 (d, B2, J_{BH} 131), −32.9 (d, B9, J_{BH} 102), −35.9 (d, B4, J_{BH} 131), −43.7 (d, B1, J_{BH} 115)
	$^1H\{^{11}B\}^{f,i,j}$	7.2 (m, br, C_6H_5), 3.79 (1, BH), 3.44 (1, BH), 2.76 (m, 2, CH_2), 2.66 (1, BH), 2.40 (1, NH), 2.13 (1, BH), 1.53 (1, CH), 1.41 (1, BH), 1.14 (1, BH), 0.70 (1, BH), 0.17 (2, BH), −1.08 (1, BH), −2.53 (1, BHB), −2.66 (1, BHB)
hypho-8-CH_3-8,13-CNB_8H_{14} (**5a**)	$^{11}B^{a,m}$	25.9 (d, B2, J_{BH} 160), −0.6 (d, B10, J_{BH} 157), −5.0 (d, B3, J_{BH} 130), −10.2 (d, B12, J_{BH} 149), −33.3 (d of t, B1, J_{BH} 153, $J_{B\mu H}$ ∼65), −39.5 (d of t, B9, J_{BH} 150, $J_{B\mu H}$ ∼40), −45.5 (d, B6, J_{BH} 146), −48.5 (d, B4, J_{BH} 144)
	^{11}B (calc)^c	from structure in Figure 20a: 40.7 (B2), 12.4 (B10), 2.1 (B3), −9.0 (B1), −23.8 (B12), −24.8 (B6), −30.2 (B9), −55.1 (B4) from structure in Figure 20b: 40.9 (B2), 13.1 (B10), −8.6 (B12), −14.4 (B3), −14.7 (B9), −29.5 (B1), −33.4 (B4), −53.2 (B6)
	$^{11}B-^{11}B^{a,b}$	observed crosspeaks: B1−B3, B1−B4, B2−B4, B2−B6, B2−B9, B3−B4, B4−B6, B4−B10, B6−B9, B6−B10, B6−B12, B9−B12
	$^1H\{^{11}B\}^{b,f,j}$	4.83 (1, BH), 3.63 (1, BH), 2.96 (1, NH), 2.79 (1, BH), 2.65 (1, BH), 1.31 (d, 4, CH_3, BH, J_{CH} 7), 1.17 (1, BH), 0.52 (1, CH), 0.36 (1, BH), 0.07 (2, BH), −0.65 (1, BH), −1.98 (1, BHB), −2.41 (1, BHB)
hypho-8-CH_3-8,13-$^{13}CNB_8H_{14}$ (**5a**-^{13}C)	$^{11}B\{^1H\}^{a,b}$	25.6 (s, B2), −0.9 (s, B10), −4.7 (d, B3, $J_{^{11}B^{13}C}$ 45), −9.7 (s, B12), −33.8 (s, B1), −39.4 (d, B9), −46.3 (s, B6), −48.8 (s, B4)
hypho-8-Bn-8,13-CNB_8H_{14} (**5b**)	$^{11}B^{a,b}$	27.9 (d, B2, J_{BH} 169), 1.9 (d, B10, J_{BH} 166), −3.2 (d, B3, J_{BH} 124), −7.3 (d, B12, J_{BH} 145), −31.6 (d, B1, J_{BH} 134), −36.9 (d, B9, J_{BH} 108), −43.9 (d, B6, J_{BH} 157), −46.6 (d, B4, J_{BH} 157)
	$^1H\{^{11}B\}^{f,j,m,n}$	7.22 (m, C_6H_5), 7.10 (m, C_6H_5), 7.05 (m, C_6H_5), 5.06 (1, BH), ∼3.9 (1, BH), 3.06 (1, BH), ∼2.4 (1, BH), 2.31 (d, CH_2, J_{HH} 7), 2.05 (1, NH), 1.61 (1, BH), 0.10 (1, BH), 0.02 (3, 2BH, CH), −0.31 (1, BH), −2.25 (1, BHB), −2.92 (1, BHB)
hypho-8-CH_3-8,13-$CNB_8H_{13}^-$ (PSH^+**5a**$^-$)	$^{11}B^{a,i}$	4.6 (d, B2, J_{BH} 133), 2.9 (d, B3, J_{BH} 102), −2.8 (d, B12, J_{BH} 125), −11.9 (d, B6, J_{BH} 127), −14.2 (d, B1, J_{BH} 133), −16.8 (d, B10, J_{BH} 142), −49.2 (d, B9, J_{BH} 100), −51.7 (d, B4, J_{BH} 114)
	^{11}B (calc)^c	8.8 (B2), 2.0 (B3), −7.4 (B12), −5.7 (B6), −10.6 (B1), −14.6 (B10), −48.4 (B9), −57.9 (B4)
	$^{11}B-^{11}B^{a,b}$	observed crosspeaks: B1−B4, B2−B6, B2−B9, B3−B4, B4−B6, B4−B10, B6−B9, B6−B10, B6−B12, B9−B12
	$^1H\{^{11}B\}^{f,i,j}$	2.74 (1, BH), 2.46 (1, BH), 2.30 (1, BH), 2.25 (1, BH), 1.94 (1, BH), 1.29 (1, BH), 1.24 (1, CH), 1.05 (d, CH_3, J_{CH} 7), −1.02 (1, BH), −1.72 (1, BH, 2, BHB), −2.32 (1, BHB)
hypho-8-CH_3-8,13-$^{13}CNB_8H_{13}^-$ (PSH^+**5a**$^{-13}$C)	$^{11}B\{^1H\}^{a,b}$	2.5 (s, B2), 1.2 (br, B3, $J_{^{11}B^{13}C}$ obscured), −5.0 (s, B12), −13.9 (s, B6), −15.5 (s, B1), −18.7 (s, B10), −51.4 (s, B9), −53.8 (s, B4)
hypho-8-Bn-8,13-$CNB_8H_{13}^-$ (PSH^+**5b**$^-$)	$^{11}B^{a,i}$	3.7 (d, B2, J_{BH} 104), 0.8 (d, B3, J_{BH} 122), −3.8 (d, B12, J_{BH} 134), −13.0 (d, B6, J_{BH} 124), −15.5 (d, B1, J_{BH} 132), −17.7 (d, B10, J_{BH} 149), −50.4 (t, B9, J_{BH} 114), −53.0 (d, B4, J_{BH} 134)

[a] 160.5 MHz. [b] CD_2Cl_2. [c] DZ/6-31G*. [d] 64.2 MHz. [e] 200.1 MHz. [f] PPN^+ or PSH^+ peaks not included. [g] 125.7 MHz. [h] Overlapped. [i] CD_3CN. [j] 500.1 MHz. [k] NH not observed. [l] Labeled carbon only. [m] C_6D_6. [n] Not all terminal BH observed.

Table 2. Crystallographic Data Collection and Structure Refinement Information

compd	PPN^+**1**$^-$	PSH^+**2a**$^-$	**3b**	PSH^+**4a**$^-$
formula	$C_{40}H_{45}P_2B_8N_2$	$B_{10}C_{16}H_{35}N_3$	$C_8B_9H_{22}N$	$C_{16}H_{36}B_9N_3$
formula wt	702.25	377.59	229.56	367.77
space group	$P\bar{1}$	$P2_1/c$	$P2_1/c$	$P2_1/c$
Z	2	4	4	4
cell constants				
a, Å	10.952(2)	12.100(3)	6.9727(4)	11.293(2)
b, Å	11.741(1)	14.306(1)	16.2462(8)	11.986(2)
c, Å	15.947(2)	14.579(3)	13.0365(7)	16.856(3)
α, deg	106.23(1)			
β, deg	82.74(1)	114.26(2)	104.513(3)	92.63(2)
γ, deg	94.39(1)			
V, Å^3	1951.3(8)	2301(2)	1429.6(1)	2279.2(7)
μ, cm^{-1}	12.28	3.91	0.52	3.97
crystal size, mm	0.15 × 0.25 × 0.38	0.08 × 0.15 × 0.35	0.45 × 0.22 × 0.20	0.45 × 0.27 × 0.050
d_{calc}, g/cm^3	1.195	1.090	1.066	1.072
radiation	Cu Kα (λ = 1.54184 Å)	Cu Kα(λ = 1.54184 Å)	Mo Kα(λ = 0.7107 Å)	Cu Kα(λ = 1.54184 Å)
θ range, deg	2.0−72.0	2.0−65.0	2.0−25.0	2.0−60.0
scan mode	ω−2θ	ω−2θ		ω−2θ
h, k, l collected	±13, +14, ±19	+14, −16, ±17	+8, ±19, ±15	+12, +13, ±17
no. of reflcns measured	8057	4291	10317	3374
no. of unique reflcns	7661	3904	2387	3205
no. of reflcns used in refinement ($F^2 > 3.0\sigma$)	6624	2728	1725	1928
no. of parameters	646	403	252	382
data/parameter ratio	10.3	6.8	6.85	5.05
R_1	0.049	0.047	0.049	0.072
R_2	0.074	0.060	0.056	0.084

Table 3. Selected Bond Distances (Å) for *arachno*-7-CH_3-5,7,14,12-$C_3NB_8H_{11}^-$ (**1**$^-$)

B1−B2	1.854(3)	B1−B3	1.774(3)	B1−B4	1.774(4)
B1−C5	1.590(4)	B1−H1	1.057(19)	B2−B3	1.782(3)
B2−B8	1.842(3)	B2−C7	1.519(3)	B2−H2	1.119(23)
B3−B4	1.768(4)	B3−B8	1.776(3)	B3−B9	1.768(4)
B3−H3	1.117(20)	B4−B9	1.765(3)	B4−B10	1.737(4)
B4−C5	1.673(3)	B4−H4	1.101(22)	B8−B9	1.775(4)
B8−C14	1.588(3)	B8−H8	1.115(18)	B9−B10	1.742(4)
B9−C14	1.676(3)	B9−H9	1.089(20)	B10−B11	1.872(4)
B10−C5	1.658(3)	B10−C14	1.642(3)	B10−H10	1.084(28)
B11−C5	1.726(3)	B11−C14	1.711(3)	B11−N12	1.495(3)
B11−H11	1.139(22)	C5−H5	1.005(21)	C7−C7a	1.514(3)
C7−N12	1.310(3)	C14−H14	0.897(27)	N12−H12	1.033(25)

Table 4. Selected Bond Distances (Å) for *arachno*-7-CH_3-7,12-$CNB_{10}H_{13}^-$ (**2a**$^-$)

B1−B2	1.927(4)	B1−B3	1.742(3)	B1−B4	1.756(4)
B1−B5	1.820(4)	B1−H1	1.016(25)	B1−H1,5	1.283(20)
B2−B3	1.751(3)	B2−B8	1.913(3)	B2−C7	1.539(3)
B2−H2	1.141(22)	B3−B4	1.770(4)	B3−B8	1.716(4)
B3−B9	1.756(4)	B3−H3	1.119(20)	B4−B5	1.728(4)
B4−B9	1.780(4)	B4−B10	1.770(4)	B4−H4	1.087(22)
B5−B10	1.717(4)	B5−B11	1.945(5)	B5−H5	1.173(20)
B5−H1,5	1.224(21)	B8−B9	1.753(4)	B8−B14	1.822(4)
B8−H8	1.111(17)	B8−H8,14	1.243(21)	B9−B10	1.763(3)
B9−B14	1.733(4)	B9−H9	1.069(17)	B10−B11	1.756(4)
B10−B14	1.708(4)	B10−H10	1.106(24)	B11−B14	1.942(3)
B11−N12	1.509(3)	B11−H11	1.151(22)	B14−H14	1.075(23)
B14−H8,14	1.263(20)	C7−C7a	1.510(3)	C7−N12	1.307(3)
N12−H12	1.012(22)				

Table 5. Selected Bond Distances (Å) for *hypho*-12-Bn-12,13-CNB_9H_{15} (**3b**)

B1−B2	1.805(4)	B1−B3	1.793(4)	B1−B4	1.731(4)
B1−B5	1.924(4)	B1−H1	1.090(21)	B1−H1,2	1.220(20)
B2−B3	1.793(3)	B2−B8	1.967(4)	B2−H1,2	1.313(20)
B2−H2	1.107(20)	B3−B4	1.764(4)	B3−B8	1.783(4)
B3−B9	1.786(4)	B3−H3	1.030(20)	B4−B5	1.750(4)
B4−B9	1.730(4)	B4−B10	1.753(4)	B4−H4	1.075(20)
B5−B10	1.775(4)	B5−B11	1.851(4)	B5−H5	1.103(22)
B5−H5,11	1.154(21)	B8−B9	1.818(3)	B8−H8,9	1.315(19)
B8−H8	1.107(19)	B9−B10	1.908(4)	B9−H8,9	1.243(20)
B9−H9	1.067(21)	B10−B11	1.853(4)	B10−H10	1.120(20)
B10−H10,11	1.180(20)	B11−H5,11	1.358(22)	B11−H11	1.107(20)
B11−H10,11	1.352(20)	C12−C14	1.537(3)	C12−B11	1.616(3)
C12−H12	0.975(20)	N13−C12	1.510(3)	N13−B2	1.551(3)
N13−B8	1.553(3)	N13−H13	0.916(24)		

Table 6. Selected Bond Distances (Å) for *hypho*-12-CH_3-12,11-$CNB_9H_{14}^-$ (**4a**$^-$)

B1−B2	1.803(11)	B1−B3	1.800(9)	B1−B4	1.804(9)
B1−B5	1.770(9)	B1−B7	1.798(12)	B1−H1	1.002(56)
B2−B3	1.727(10)	B2−B7	1.817(11)	B2−B8	1.869(10)
B2−H2	1.044(54)	B2−H2,7	1.288(43)	B3−B4	1.752(9)
B3−B8	1.683(10)	B3−B9	1.706(10)	B3−H3	1.001(60)
B4−B5	1.758(8)	B4−B9	1.754(10)	B4−B10	1.743(9)
B4−H4	1.176(47)	B5−B10	1.912(9)	B5−H5	1.161(47)
B7−H7	1.116(50)	B7−H2,7	1.455(41)	B8−B9	1.865(10)
B8−H8a	1.137(47)	B8−H8b	1.164(59)	B9−B10	1.821(9)
B9−H9	1.052(54)	B9−H9,10	1.384(48)	B10−H10	1.233(50)
B10−H9,10	1.479(48)	N11−C12	1.463(7)	N11−B5	1.547(9)
N11−B10	1.544(7)	C12−C12a	1.527(8)	C12−B7	1.612(11)
C12−H12	1.185(77)				

simple skeletal electron counting rules,[16] the compounds should then adopt cage structures based on a 14-vertex bicapped hexagonal antiprism missing two vertices. Indeed, the observed structures can be derived in this manner, as shown in Figure 3, by removal of the number 6 and 13 vertices. Alternatively, the −MeC═NH− groups may be viewed as exopolyhedral substituents bridging the B2 and B11 atoms on open 10-vertex arachno frameworks, i.e. *arachno*-$\mu_{2,11}$-(MeC═NH)-5,14-$C_2B_8H_{10}^-$ and *arachno*-$\mu_{2,11}$-(MeC═NH)-$B_{10}H_{12}^-$. The −MeC═NH− fragment could then be considered to be connected to the boron cage by a 2-electron covalent bond between B2 and C7 and a 2-electron coordinate-covalent bond from N12 to B11. In this view, the compounds would be considered imine-bridged analogs of *arachno*-6-NMe_3-5,7-$C_2B_8H_{12}$,[17] *arachno*-6,9-$L_2B_{10}H_{12}$,[18] or *arachno*-$B_{10}H_{14}^{2-}$.[19] This interpretation is supported by the C7−N12 bond distances, which are within

(16) (a) Williams, R. E. *Inorg. Chem.* **1971**, *10*, 210−214. (b) Wade, K. *Adv. Inorg. Chem. Radiochem.* **1976**, *18*, 1−66. (c) Williams, R. E. *Adv. Inorg. Chem. Radiochem.* **1976**, *18*, 67−142. (d) Rudolph, R. W. *Acc. Chem. Res.* **1976**, *9*, 446−452.

(17) Garrett, P. M.; Ditta, G. S.; Hawthorne, M. F. *J. Am. Chem. Soc.* **1971**, *93*, 1265−1266.

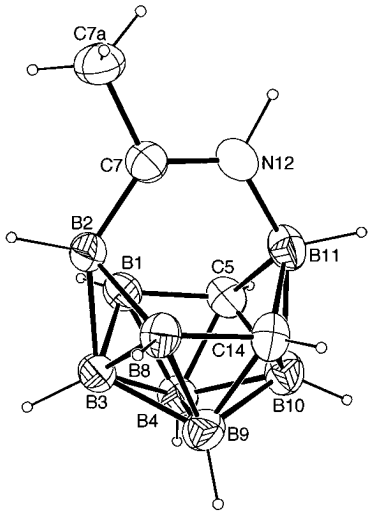

Figure 1. ORTEP drawing of the molecular structure of *arachno*-7-CH_3-5,7,14,12-$C_3NB_8H_{11}^-$ (**1**$^-$).

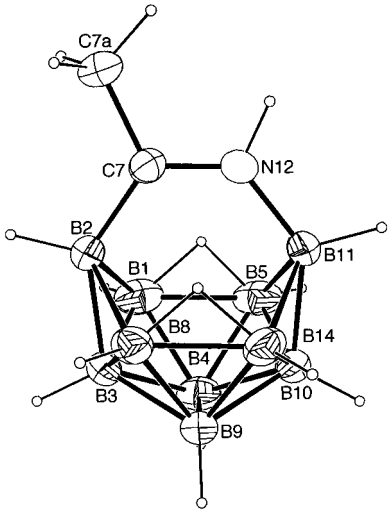

Figure 2. ORTEP drawing of the molecular structure of *arachno*-7-CH_3-7,12-$CNB_{10}H_{13}^-$ (**2a**$^-$).

the normal range for carbon−nitrogen double bonds, and the bond angles around the C7 center (e.g. for **1**$^-$, B2−C7−C7a, 120.0(2)°; B2−C7−N12, 123.9(2)°; C7a-C7-N12, 116.0(2)°) which suggest C7 sp^2 hybridization.

The structures of anions **1**$^-$ and **2a**$^-$ are also confirmed by ab initio/IGLO/NMR calculations.[15] In these calculations, the geometry of the proposed structure is first optimized using ab initio theory. The bond distances and angles of the optimized structure can then be compared to the values determined by X-ray crystallography, and, as shown in Tables S2a and S5a in the supporting information, the calculated bond lengths for **1**$^-$ and **2a**$^-$ are in agreement with those determined by X-ray crystallography (Tables 3 and 4). Additionally, the optimized structure can then be used as input for an IGLO NMR chemical shift calculation. This then yields ^{11}B NMR chemical shifts and assignments that can be compared to the experimentally determined chemical shifts and assignments. The experimental ^{11}B NMR spectrum of **1**$^-$ consists of six doublets in a 2:1:1:1:1:2 ratio, indicating C_s symmetry. The doublet at −20.9 ppm

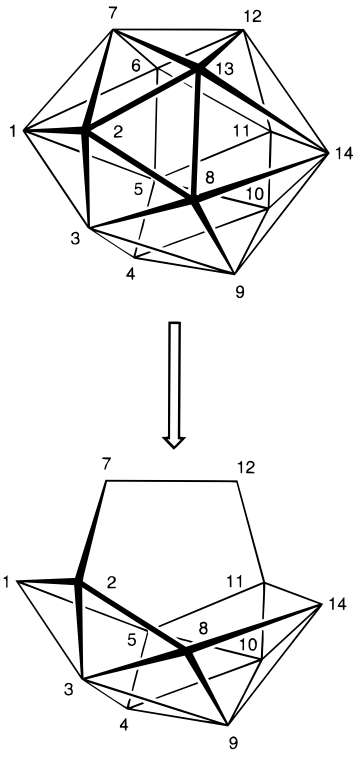

Figure 3. Derivation of the observed 12-vertex arachno structures of **1**$^-$ and **2**$^-$ from a 14-vertex bicapped hexagonal antiprism.

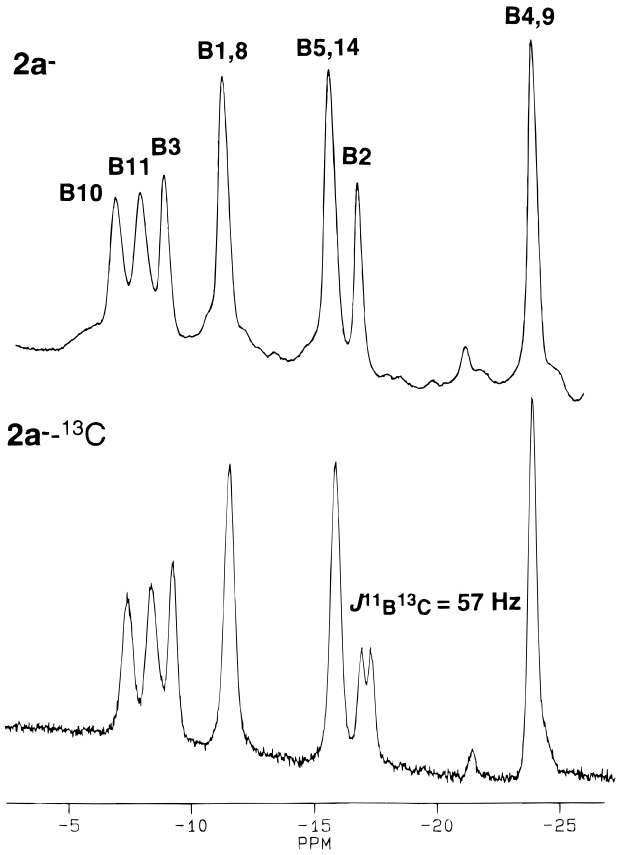

Figure 4. The ^{11}B{^{1}H} NMR spectra of *arachno*-7-CH_3-7,12-$^{13}CNB_{10}H_{13}^-$ (**2a**$^-$-^{13}C) and *arachno*-7-CH_3-7,12-$CNB_{10}H_{13}^-$ (**2a**$^-$).

is unusually sharp and shows no crosspeaks with other resonances in the 2-D ^{11}B−^{11}B NMR spectrum, suggesting that it is a boron located between two carbons. The ^{11}B NMR spectrum of **2a**$^-$ (Figure 4) at 160.5 MHz exhibits seven doublets in a 1:1:1:2:2:1:2 ratio, consistent with a C_s symmetry

(18) (a) Reddy, J. van der Mass; Lipscomb, W. N. *J. Chem. Phys.* **1959**, *31*, 610−616. (b) Reddy, J. van der Mass; Lipscomb, W. N. *J. Am. Chem. Soc.* **1959**, *81*, 754. (c) Sands, D. E.; Zalkin, A. *Acta Crystallogr.* **1962**, *15*, 410−417.

(19) Kendall, D. S.; Lipscomb, W. N. *Inorg. Chem.* **1973**, *12*, 546−551.

for the cage. As shown in Table 1, the calculated ^{11}B NMR shifts and assignments for **1**$^-$ and **2a**$^-$ are in good agreement with both the experimental ^{11}B NMR shifts and the crosspeaks found in the 2-D ^{11}B−^{11}B NMR spectra of these anions.

Further confirmation of the chemical shift assignments for **2a**$^-$ was obtained in the ^{11}B NMR spectrum of *arachno*-7-CH_3-7,12-$^{13}CNB_{10}H_{13}^-$ (**2a**$^-$-^{13}C), which was readily synthesized by the reaction of *nido*-$B_{10}H_{13}^-$ with ^{13}C-labeled acetonitrile (eq 5).

$$\textit{nido}\text{-}B_{10}H_{13}^- + CH_3{}^{13}CN \rightarrow \textit{arachno}\text{-}7\text{-}R\text{-}7,12\text{-}{}^{13}CNB_{10}H_{13}^- \quad (5)$$
(**2a**$^-$-^{13}C)

The IGLO NMR calculation and the 2-D ^{11}B−^{11}B NMR spectrum predict that the resonance at −17.1 ppm should be due to the boron (B2) that is directly attached to the nitrile carbon. A comparison of the ^{11}B{^{1}H} NMR spectra of **2a**$^-$-^{13}C with that of the unlabeled **2a**$^-$, Figure 4, shows that this resonance in the spectrum of **2a**$^-$-^{13}C does, indeed, have ^{11}B^{13}C coupling consistent with this assignment. The magnitude of this coupling constant, 57 Hz, is in the range of those reported in other polyhedral boranes and carboranes, including, $J_{^{11}B^{13}C}$ = ∼41 Hz for *nido*-6-CH_3-6-^{13}C-5,6,9-$C_3B_7H_{10}$,[9] $J_{^{11}B^{13}C}$ = 74 Hz for *nido*-1-$^{13}CH_3$-B_5H_8, and $J_{^{11}B^{13}C}$ = 64 Hz for *nido*-2-$^{13}CH_3$-B_5H_8.[20] Likewise, the proton-coupled ^{13}C NMR spectrum of **2a**$^-$ exhibits a quartet assigned to the Me and a broad singlet assigned to the C7 carbon, while the spectrum of **2a**$^-$-^{13}C exhibits a quartet for the C7 carbon, with $J_{^{13}C^{11}B}$ = 60 Hz.

The other spectral data obtained for **1**$^-$ and **2a**$^-$ also support their formulations. The ^{1}H NMR spectrum for **1**$^-$ shows a singlet for the methyl at 2.43 ppm and two broad resonances at 6.46 and 1.55 ppm, which are assigned to the NH and terminal C5,14 protons, respectively. Its proton-coupled ^{13}C NMR spectrum exhibits a quartet, doublet, and broad singlet arising from the Me, C5,14, and C7 carbons, respectively. The ^{1}H{^{11}B} NMR spectrum of **2a**$^-$ shows, in addition to the terminal BH resonances, a broad resonance at 8.33 ppm and singlets at 2.27 and −8.08 ppm, which are assigned to the NH, Me, and bridge hydrogens, respectively. The presence of an NH group in both compounds is likewise supported by IR stretches at 3360 cm^{-1} for PPN$^+$**1**$^-$ and 3310 cm^{-1} for PSH$^+$**2a**$^-$.

The formation of **1**$^-$ and **2**$^-$ can be envisioned to occur by a reaction sequence similar to that originally proposed for the reactions of acetonitrile with the *arachno*-6,8-$C_2B_7H_{12}^-$ and *arachno*-6,8-$S_2B_7H_8^-$ anions. Thus, as shown in Figure 5 for the reaction with *nido*-$B_{10}H_{13}^-$, a sequence involving the initial nucleophilic attack at the positive nitrile carbon followed by nitrile hydroboration would produce an imino intermediate. Such a species would be highly nucleophilic and the insertion of this unit in the manner shown is consistent with the electrophilic nature of the 6,9-borons in the decaborane framework.[21]

The formation of **1**$^-$ also involves other cage rearrangements during insertion of the nitrile group. As shown in Figure 1, the cage carbon atoms, C5 and C14, in **1**$^-$ are non-adjacent, in contrast to their adjacent positions in the starting *nido*-5,6-$C_2B_8H_{11}^-$. If, as shown in Figure 6, insertion of the nitrile were to occur without skeletal rearrangement, then the adjacent-carbon *arachno*-7-CH_3-5,7,11,12-$C_3NB_8H_{11}^-$ would be produced. However, ab initio calculations show that this structure is 57 kcal/mol higher in energy than *arachno*-7-CH_3-5,7,14,12-$C_3NB_8H_{11}^-$.

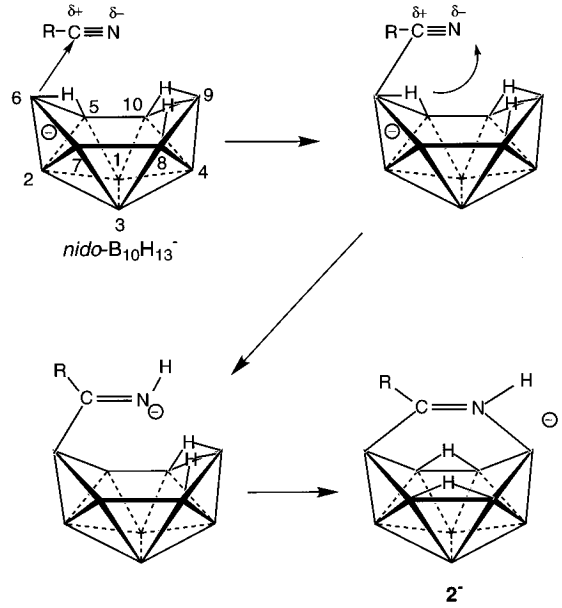

Figure 5. Possible reaction sequence leading to the formation of *arachno*-7-CH_3-7,12-$CNB_{10}H_{13}^-$ (**2a**$^-$) in the reaction of *nido*-$B_{10}H_{13}^-$ with acetonitrile.

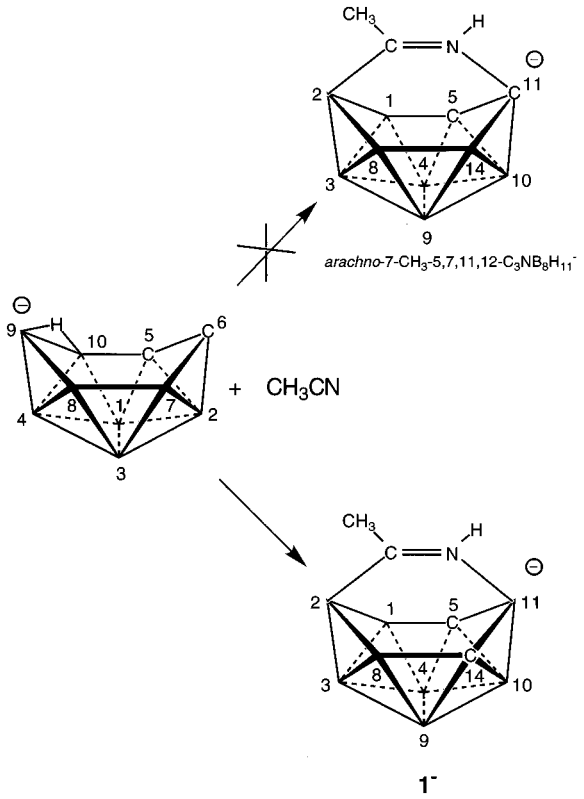

Figure 6. Cage carbon rearrangement in the reaction of *nido*-5,6-$C_2B_8H_{11}^-$ with acetonitrile to form *arachno*-7-CH_3-5,7,14,12-$C_3NB_8H_{11}^-$ (**1**$^-$).

The mechanism of carbon rearrangement is unclear, but similar rearrangements of cage carbons in 10-vertex dicarbaborane structures have also been observed during thermolytic dehydrogenation (at 200 °C) of *arachno*-5,6-$C_2B_8H_{12}^{2-}$, which produced *nido*-5,7-$C_2B_8H_{10}^{2-}$.[22]

A comparison of the reactions in eqs 1, 3, and 4 with that of eq 2 demonstrates that nitriles react with polyhedral borane anions in two distinct ways. The reactions of the *arachno*-6,8-

(20) Onak, T.; Wan, E. *J. Magn. Reson.* **1974**, *14*, 66−71.

(21) (a) Su, K.; Barnum, B.; Carroll, P. J.; Sneddon, L. G. *J. Am. Chem. Soc.* **1992**, *114*, 2730−2731. (b) Su, K.; Carroll, P. J.; Sneddon, L. G. *J. Am. Chem. Soc.* **1993**, *115*, 10004−10017.

(22) Štíbr, B.; Plešek, J.; Heřmánek, S. *Collect. Czech., Chem. Commun.* **1973**, *38*, 338−342.

$S_2B_7H_8^-$ (eq 1), *nido*-5,6-$C_2B_8H_{11}^-$ (eq 3), and *nido*-$B_{10}H_{13}^-$ (eq 4) anions with nitriles result in carbon and nitrogen insertion to yield azacarborane products. In contrast, the reaction of acetonitrile with *arachno*-6,8-$C_2B_7H_{12}^-$ (eq 2) results in deammination and monocarbon insertion to produce the tricarbaborane *nido*-6-CH_3-5,6,9-$C_3B_7H_9^-$. The differences in reactivity may be related to either the relative basicities of the imine nitrogens or the number of hydrogens in the borane or carborane cages that are available for further reduction of the imine bond. In *arachno*-6,8-$C_2B_7H_{12}^-$ there are two additional acidic hydrogens, and the observed product is consistent with the complete reduction of the imine and loss of NH_3, with the carbon from the acetonitrile then inserting into the cage to yield the tricarbaborane. In *arachno*-6,8-$S_2B_7H_8^-$, $\mathbf{1}^-$, and $\mathbf{2}^-$ there are not sufficient hydrogens present to allow for both deammination and the generation of a stable cage fragment without extensive framework rearrangement. These observations suggested that deammination could perhaps be induced in these anions under acidic conditions.

Although attempts to acidify both $PPN^+\mathbf{1}^-$ and $PSH^+\mathbf{2}^-$ with HCl/Et_2O gave no reaction, the two phase reaction[23] of PPN^+-*arachno*-7-CH_3-5,7,14,12-$C_3NB_8H_{11}^-$ ($PPN^+\mathbf{1}^-$) with H_2SO_4 and CH_2Cl_2 resulted in loss of a "H_2BN" unit from the cage and further insertion of the nitrile carbon to form the known tricarbaborane, *nido*-6-CH_3-5,6,9-$C_3B_7H_{10}$, in 41.5% yield, as shown in eq 6. The product was identified by its spectral data

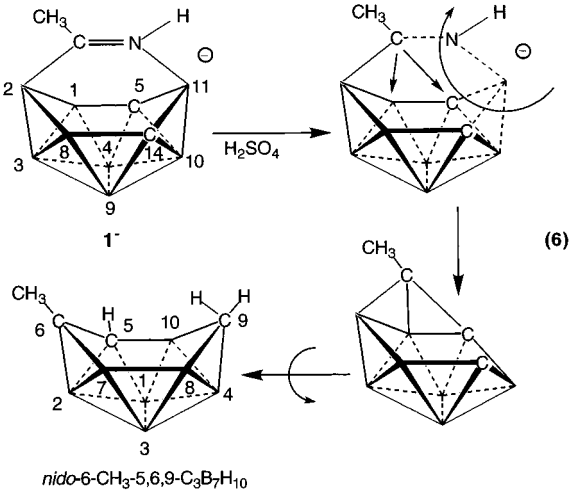

as the tricarbaborane previously generated by acidification of the anion obtained from the reaction of *arachno*-6,8-$C_2B_7H_{12}^-$ and acetonitrile.[6] Thus, the reaction of $\mathbf{1}^-$ with H_2SO_4 provides another synthetic route to this tricarbaborane.

In contrast to the reaction above, the acidification of PSH^+-*arachno*-7-R-7,12-$CNB_{10}H_{13}^-$ ($PSH^+\mathbf{2a}^-$, $PSH^+\mathbf{2b}^-$, $PSH^+\mathbf{2a}^-$-^{13}C) with H_2SO_4 was found to result in loss of only one cage boron, producing the *hypho*-12-R-12,13-CNB_9H_{15} (**3a**, **3b**, **3a**-^{13}C) (eq 7) azamonocarbaboranes.

$$\begin{array}{c} PSH^+\textit{arachno}\text{-7-R-7,12-}CNB_{10}H_{13}^- \xrightarrow[CH_2Cl_2]{H_2SO_4} \\ (R = CH_3,\ \mathbf{2a}^-;\ \mathbf{2a}^-\text{-}^{13}C) \\ (R = Bn,\ \mathbf{2b}^-) \\ \textit{hypho}\text{-12-R-12,13-}CNB_9H_{15} \\ (R = CH_3,\ \mathbf{3a};\ \mathbf{3a}\text{-}^{13}C) \\ (R = Bn,\ \mathbf{3b}) \end{array} \quad (7)$$

(23) (a) Štíbr, B. Private communication. (b) Holub, J.; Wille, A. E.; Štíbr, B.; Carroll, P. J.; Sneddon, L. G. *Inorg. Chem.* **1994**, *33*, 4920−4926.

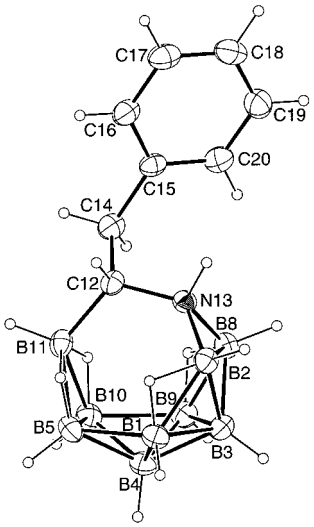

Figure 7. ORTEP drawing of the molecular structure of *hypho*-12-Bn-12,13-CNB_9H_{15} (**3b**).

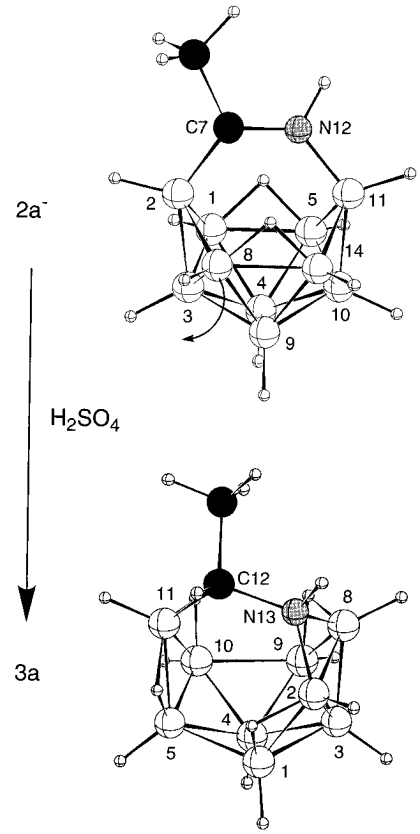

Figure 8. Comparison of the structures of $\mathbf{2a}^-$ and **3a**.

The products were isolated in low yields as air-sensitive white solids. A single-crystal X-ray study of *hypho*-12-Bn-12,13-CNB_9H_{15} (**3b**) confirmed the open cage structure shown in Figure 7. As shown in Figure 8, the boron framework in this structure may be generated in a straightforward manner by removal of the B8 (or B1) boron of $\mathbf{2a}^-$. However, in contrast to the structures observed for $\mathbf{1}^-$ and $\mathbf{2a}^-$, the −CH(Bn)NH═ unit in **3b** is bridging between three borons with the carbon attached to B11 and the nitrogen bridging the B2−B8 edge. Furthermore, an additional hydrogen is present at C12 and the C12−N13 distance of 1.510(3) Å, along with the bond angles around the tetracoordinate C12 carbon (B11−C12−N13, 117.1(2)°; B11−C12−C14, 111.0(2)°; C14−C12−N13, 108.4(2)°), are consistent with a carbon−nitrogen single bond (Table 5). The molecule contains two six-membered open faces,

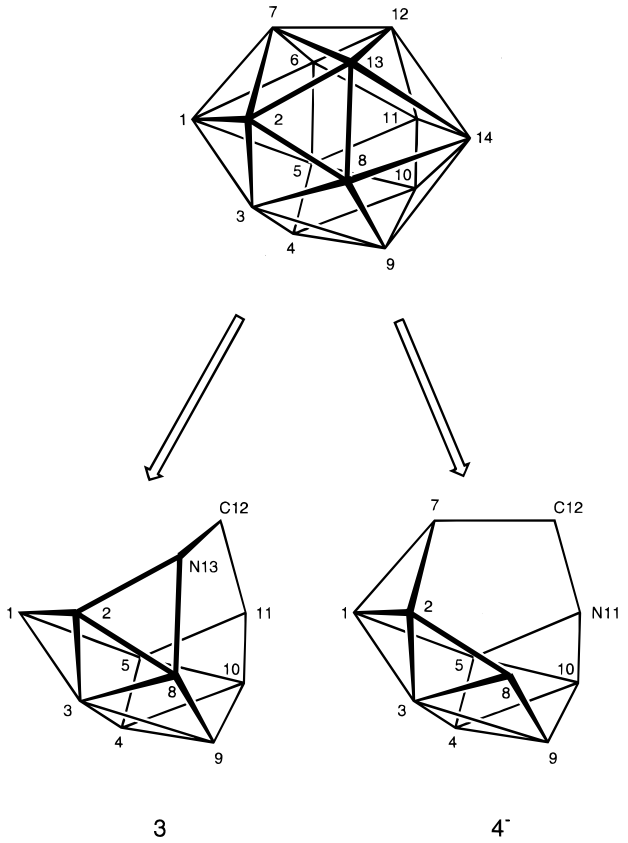

Figure 9. Derivation of the observed and proposed 11-vertex hypho structures of **3** and $\mathbf{4}^-$ from a bicapped hexagonal antiprism.

one on either side of the bridging −CH(Bn)NH═ unit. There are four bridge hydrogens, two located on the B5−B11 and B10−B11 edges and two others on the B1−B2 and B8−B9 edges.

The structure observed for **3** is consistent with that expected for an 11-vertex hypho cluster (n+4 skeletal electron pairs), and may be derived from a 14-vertex bicapped hexagonal antiprism by removing the number 6, 7, and 14 vertices, as shown in Figure 9. One other 11-vertex hypho cage, the *hypho*-5-CH_3-5,11,7,14-$CNS_2B_7H_9$, has been previously isolated, but it has a different 11-vertex hypho structure, which is derived from the bicapped hexagonal antiprism by removing the number 6, 10, and 13 vertices.[6] Alternatively, as described above for $\mathbf{1}^-$ and $\mathbf{2}^-$, if the −CH(R)NH═ group is considered as only an exopolyhedral unit, then **3** can be considered to be a 9-vertex arachno framework with the −CH(R)NH═ unit bridging the cage. As shown in Figure 10, **3** has the same boron skeletal framework as observed for *n*-B_9H_{15}.[24] Comparison of the X-ray determined structures of *n*-B_9H_{15} and **3b** shows that they have similar distances and angles. The one major difference is that in **3b** the B2−B11 and B8−B11 distances (∼3.30 Å) are significantly shorter than the corresponding distances in *n*-B_9H_{15} (∼3.92 Å) and the B9−B10−B11 and B8−B9−B10 angles are smaller in **3b** (109.8(2)° and 114.7(2)°) than in *n*-B_9H_{15} (∼119.3° and ∼125.1°). These differences are undoubtedly due to the bridging CN unit in **3b**, which requires shortening of the B2−B11 and B8−B11 bond distances.

The structure of **3** is also supported by ab initio/IGLO/NMR calculations on **3a**. The calculated bond lengths of **3a** are in good agreement with those crystallographically determined for **3b**, as shown in Table S8a in the supporting information. In the $^{11}B\{^1H\}$ NMR spectrum of **3a**, shown in Figure 11, there are eight boron resonances, one of intensity two, and two other pairs of resonances which are closely space together. This is expected, as it is only the two different substituents on the C12 carbon that disrupt the mirror symmetry of the cage. The calculated ^{11}B NMR chemical shifts are in good agreement with the experimental spectrum, as shown in Table 1. The $^{11}B\{^1H\}$ NMR spectrum of (**3a**-^{13}C) (Figure 11) shows a $J_{^{11}B^{13}C}$ of 53 Hz, on the resonance at 4.1 ppm, confirming the assignment of the B11 resonance. Likewise, the ab initio/IGLO/NMR predicted chemical shifts and assignments agree with those determined from the 2-D $^{11}B-^{11}B$ NMR spectrum.

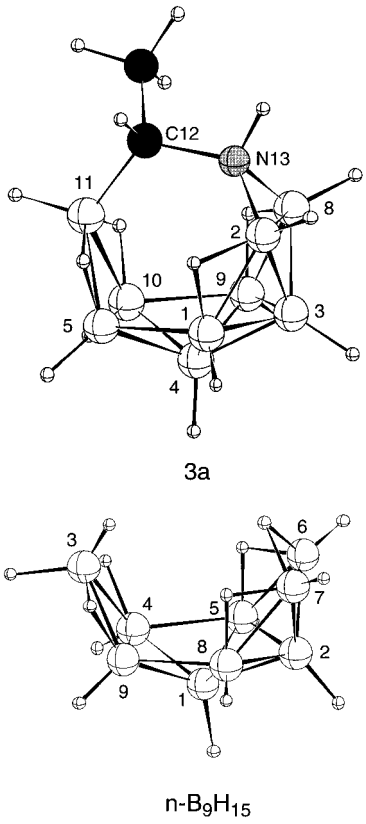

Figure 10. Comparison of the structures of **3a** and *n*-B_9H_{15}.

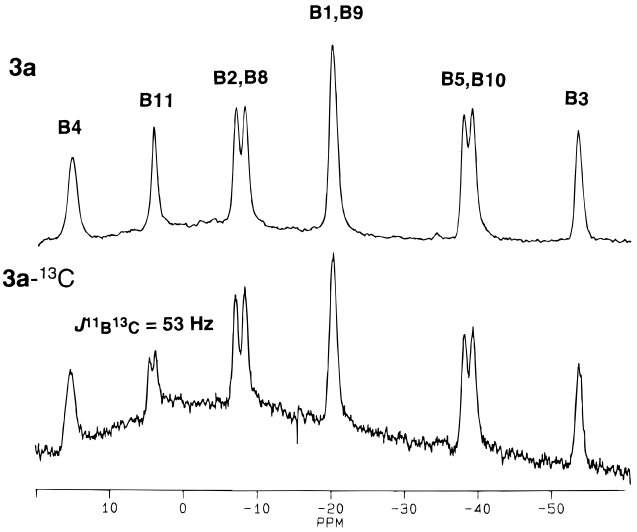

Figure 11. The $^{11}B\{^1H\}$ NMR spectra of *hypho*-12-CH_3-12,13-$^{13}CNB_9H_{15}$ (**3a**-^{13}C) and *hypho*-12-CH_3-12,13-CNB_9H_{15} (**3a**).

(24) (a) Dickerson, R. E.; Wheatley, P. J.; Howell, P. A.; Lipscomb, W. N. *J. Chem. Phys.* **1957**, *27*, 200−209. (b) Simpson, P. G.; Lipscomb, W. N. *J. Chem. Phys.* **1961**, *35*, 1340−1343. (c) Beaudet, R. A. In *Advances in Boron and the Boranes*; Liebman, J. F., Greenberg, A., Williams, R. E., Eds.; VCH Publishers: New York, 1988; pp 417−490.

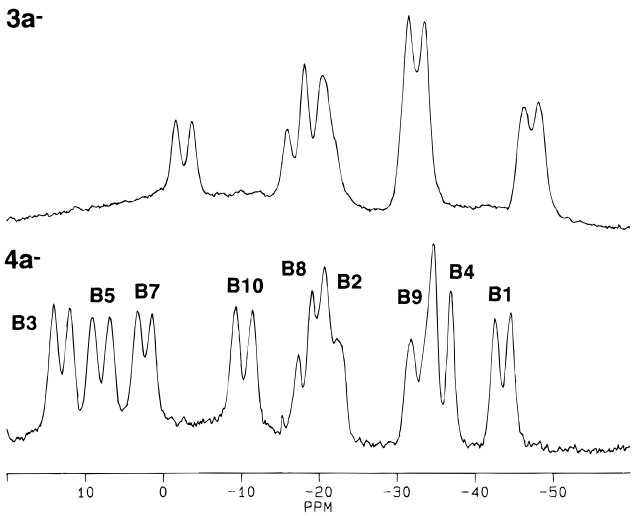

Figure 12. The 64.2-MHz ^{11}B proton coupled NMR spectra of **3a**$^-$ and **4a**$^-$.

The deprotonation of **3a**, **3b**, and **3a**-^{13}C with Proton Sponge initially yields PSH$^+$-*hypho*-12-R-12,13-$CNB_9H_{14}^-$ (PSH$^+$**3a**$^-$, PSH$^+$**3b**$^-$, PSH$^+$**3a**$^-$-^{13}C) (eq 8). This anion is unstable at room temperature and completely isomerizes to a second borane anion, PSH$^+$-*hypho*-12-R-12,11-$CNB_9H_{14}^-$ (PSH$^+$**4a**$^-$, PSH$^+$**4b**$^-$, PSH$^+$**4a**$^-$-^{13}C) after the solution is stirred for 24 h (eq 9).

$$\begin{aligned} &\textit{hypho}\text{-12-R-12,13-}CNB_9H_{15} + PS \xrightarrow{CH_2Cl_2} \\ &\quad (R = CH_3,\ \mathbf{3a};\ \mathbf{3a}\text{-}^{13}C) \\ &\quad\quad (R = Bn,\ \mathbf{3b}) \\ &\quad\quad\quad PSH^+\text{-}\textit{hypho}\text{-12-R-12,13-}CNB_9H_{14}^- \\ &\quad\quad\quad\quad (R = CH_3,\ \mathbf{3a}^-;\ \mathbf{3a}^-\text{-}^{13}C) \\ &\quad\quad\quad\quad\quad (R = Bn,\ \mathbf{3b}^-) \end{aligned} \tag{8}$$

$$\begin{aligned} &PSH^+\text{-}\textit{hypho}\text{-12-R-12,13-}CNB_9H_{14}^- \xrightarrow[24\ h]{CH_2Cl_2} \\ &\quad (R = CH_3,\ \mathbf{3a}^-;\ \mathbf{3a}^-\text{-}^{13}C) \\ &\quad\quad (R = Bn,\ \mathbf{3b}^-) \\ &\quad\quad\quad PSH^+\text{-}\textit{hypho}\text{-12-R-12,11-}CNB_9H_{14}^- \\ &\quad\quad\quad\quad (R = CH_3,\ \mathbf{4a}^-;\ \mathbf{4a}^-\text{-}^{13}C) \\ &\quad\quad\quad\quad\quad (R = Bn,\ \mathbf{4b}^-) \end{aligned} \tag{9}$$

The significant differences observed in the ^{11}B NMR spectra of these two anions (Figure 12) suggest that they have very different skeletal arrangements. If the anion (PSH$^+$**3a**$^-$, PSH$^+$**3b**$^-$, PSH$^+$**3a**$^-$-^{13}C) is reprotonated with HCl/Et_2O before rearrangement, the initial neutral product (**3a**, **3b**, **3a**-^{13}C) is regenerated (eq 10).

$$\begin{aligned} &PSH^+\text{-}\textit{hypho}\text{-12-R-12,13-}CNB_9H_{14}^- \xrightarrow{HCl/Et_2O} \\ &\quad (R = CH_3,\ \mathbf{3a}^-;\ \mathbf{3a}^-\text{-}^{13}C) \\ &\quad\quad (R = Bn,\ \mathbf{3b}^-) \\ &\quad\quad\quad \textit{hypho}\text{-12-R-12,13-}CNB_9H_{15} \\ &\quad\quad\quad\quad (R = CH_3,\ \mathbf{3a};\ \mathbf{3a}\text{-}^{13}C) \\ &\quad\quad\quad\quad\quad (R = Bn,\ \mathbf{3b}) \end{aligned} \tag{10}$$

The reversibility of the initial deprotonation suggests that the anion (**3a**$^-$, **3b**$^-$, **3a**$^-$-^{13}C) retains the same boron framework as in **3a**, **3b**, and **3a**-^{13}C. In contrast, after the cage rearrangement the new anion (PSH$^+$**4a**$^-$, PSH$^+$**4b**$^-$, PSH$^+$**4a**$^-$-^{13}C) is unreactive to HCl/Et_2O, and reaction with H_2SO_4 results in cage degradation as described later.

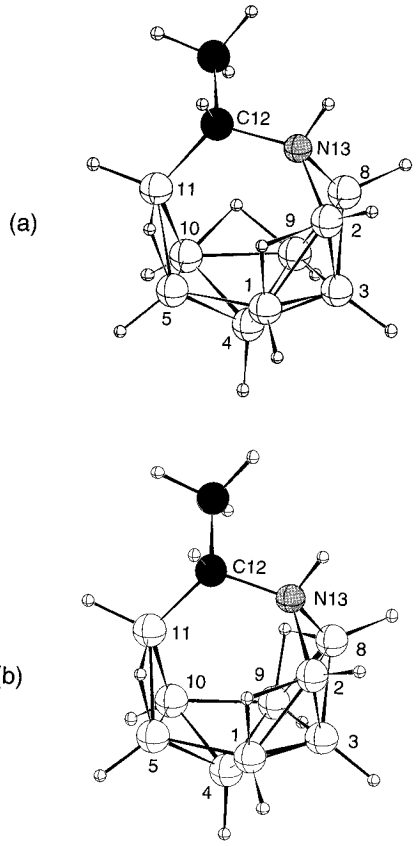

Figure 13. Comparison of the two calculated structures of **3a**$^-$.

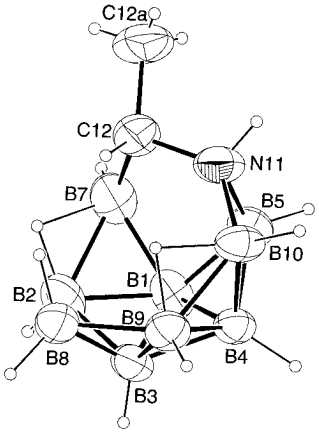

Figure 14. ORTEP drawing of the molecular structure of *hypho*-12-CH_3-12,11-$CNB_9H_{14}^-$ (**4a**$^-$).

The structure of **3a**$^-$ was investigated using the ab initio/IGLO/NMR calculations. Consistent with the structural determinations of **3b** (Figure 7), in **3a** there are two sets of bridge hydrogens, with one set bridging the B5−B11 and B10−B11 edges, and the other set at the B1−B2 and B8−B9 edges. Optimization of an initial anion structure formed by removal of a proton from the B8−B9 edge in **3a** yielded the structure for **3a**$^-$ shown in Figure 13a, in which the boron framework is unchanged, but the bridge hydrogen initially on the B10−B11 edge has optimized at a bridging position on the B9−B10 edge. Optimization of the initial structure generated by the removal of a bridge hydrogen from the B10−B11 edge in **3a** yielded a different structure, shown in Figure 13b, that is only ∼0.5 kcal/mol lower in energy. The calculated ^{11}B NMR chemical shifts of both structures roughly agree with the experimental data, as shown in Table 1, but the structure in Figure 13a gives better agreement since it predicts that the resonance calculated at −20.7 ppm is the B11 boron. Thus, although overlapping

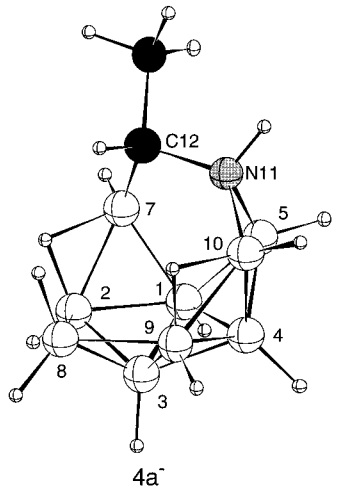

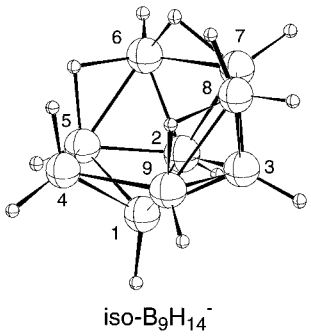

Figure 15. Comparison of the structures of **4a**$^-$ and iso-$B_9H_{14}^-$.

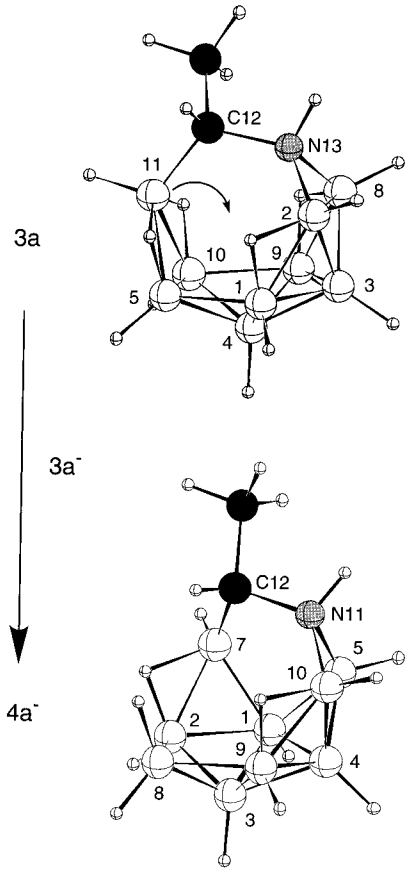

Figure 16. Comparison of the structures of **3a** and **4a**$^-$.

resonances in the 2-D $^{11}B-^{11}B$ NMR spectrum do not allow complete assignment of the boron resonances, the $^{11}B\{^1H\}$ NMR spectrum of **3a**$^-$-^{13}C confirms the resonance at −19.0 ppm as due to B11, since it is the only resonance exhibiting $^{11}B-^{13}C$ coupling. Possible fluxional behavior of **3a**$^-$ in solution is suggested by the closeness in energy of the two optimized structures and its ^{11}B NMR spectrum, which has several broad resonances. Because of this, the exact location of the bridge and/or endo hydrogens in **3a**$^-$ cannot be determined with confidence based upon the experimental and calculated data.

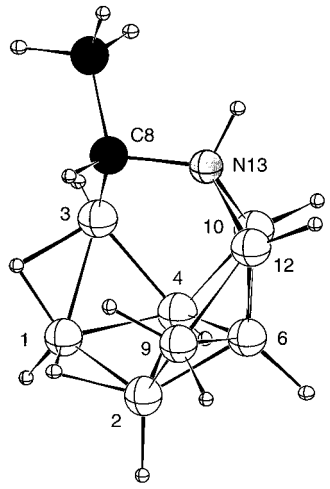

Figure 17. Proposed structure for *hypho*-8-CH_3-8,13-$CNB_8H_{13}^-$ (**5a**$^-$).

As discussed above, upon standing at room temperature in solution, **3**$^-$ quantitatively isomerizes to **4**$^-$ (eq 9). The structure of **4a**$^-$ was determined by a single-crystal X-ray study, as shown in the ORTEP drawing in Figure 14. As found for **3b**, **4a**$^-$ also has a structure based on an 11-vertex hypho geometry, but it has a different arrangement of the cage borons than found in **3b**. The structure of **4a**$^-$ can be derived from the bicapped hexagonal antiprism by removing the number 6, 13, and 14 vertices, as shown in Figure 8. The $-CH(CH_3)NH=$ unit in **4a**$^-$, as in **3b**, is still bridging three boron atoms, with the carbon attached to B7 and the nitrogen attached to B5 and B10. In contrast to **3b**, which has two six-membered open faces, in **4a**$^-$ there is one five-membered (B1−B7−C12−N11−B5) and one seven-membered (B8−B2−B7−C12−N11−B10−B9) open faces. Two bridge hydrogens are located on the seven-membered face, bridging B2−B7 and B9−B10, and there is also an endo-BH at B8. The observed structure is also supported by ab initio/IGLO/NMR calculations, which are in good agreement (Table S11a, supporting information) with both the observed bond lengths (Table 6) and the experimental ^{11}B NMR chemical shifts and assignments (Table 1) of **4a**$^-$. The $^{11}B\{^1H\}$ NMR spectrum of (**4a**$^-$-^{13}C) shows broadening of the B7 resonance, consistent with $^{11}B-^{13}C$ coupling. This assignment agrees with both the 2-D $^{11}B-^{11}B$ NMR spectrum and the ab initio/IGLO/NMR calculations.

Again, as discussed above for **3**, if the CN atoms are considered as only an exopolyhedral unit, then **4**$^-$ can be considered to be a 9-vertex arachno borane cluster with a bridging $-CH(R)NH=$ unit. However, in contrast to **3**, **4**$^-$ has a boron framework based on the iso-9-vertex arachno geometry. The "iso" type of 9-vertex arachno framework is much more common than the "normal"-9-vertex framework observed for *n*-B_9H_{15}.[24] The boron cage framework of **4a**$^-$ is similar to that determined crystallographically for *arachno*-B_9H_{13}•CH_3CN[25]

(25) (a) Wang, F. E.; Simpson, P. G.; Lipscomb, W. N. *J. Am. Chem. Soc.* **1961**, *83*, 491−492. (b) Wang, F. E.; Simpson, P. G.; Lipscomb, W. N. *J. Chem. Phys.* **1961**, *35*, 1335−1339.

and iso-$B_9H_{14}^-$,[26] as shown in Figure 15. The major difference in the structures is that **4a**$^-$ has a more open cage as a result of the bridging unit, which forces the B5−B7 bond in **4a**$^-$ to lengthen to ∼2.30 Å, compared to the analogous B6−B7 bond (∼1.79 Å) of iso-$B_9H_{14}^-$. The boron skeletal rearrangement in converting **3** to **4**$^-$ can be accomplished, as shown in Figure 16, by movement of B11 in **3** from a position on the B5−B10 edge to a position on the B9−B10 edge. The boron skeletal rearrangement that occurs during the isomerization of **3**$^-$ to **4**$^-$ is consistent with a similar rearrangement that is observed when *n*-B_9H_{15} is deprotonated by NH_3 to yield *n*-$B_9H_{14}^-$, which then rapidly rearranges to iso-$B_9H_{14}^-$ at room temperature.[27]

Protonation of **4**$^-$ should yield an isomer of **3** with an iso-B_9H_{15} boron framework, but it was found that the reaction of (PSH^+**4a**$^-$, PSH^+**4b**$^-$, PSH^+**4a**$^-$-^{13}C) with H_2SO_4 results in further cage degradation involving loss of a boron to yield *hypho*-8-R-8,13-CNB_8H_{14} (**5a**, **5b**, **5a**-^{13}C) (eq 11). Subsequent deprotonation of this product (eq 12) yielded the 10-vertex anion PSH^+-*hypho*-8-R-8,13-$CNB_8H_{13}^-$ (PSH^+**5a**$^-$, PSH^+**5b**$^-$, PSH^+**5a**$^-$-^{13}C).

$$\begin{array}{l} PSH^+\text{-}hypho\text{-12-R-12,11-}CNB_9H_{14}^- \xrightarrow[CH_2Cl_2]{H_2SO_4} \\ \quad (R = CH_3,\ \mathbf{4a}^-;\ \mathbf{4a}^-\text{-}^{13}C) \\ \quad\quad (R = Bn,\ \mathbf{4b}^-) \end{array} \quad \begin{array}{l} hypho\text{-8-R-8,13-}CNB_8H_{14} \\ (R = CH_3,\ \mathbf{5a};\ \mathbf{5a}\text{-}^{13}C) \\ (R = Bn,\ \mathbf{5b}) \end{array} \qquad (11)$$

$$\begin{array}{l} hypho\text{-8-R-8,13-}CNB_8H_{14} + PS \rightarrow \\ \quad (R = CH_3,\ \mathbf{5a};\ \mathbf{5a}\text{-}^{13}C) \\ \quad\quad (R = Bn,\ \mathbf{5b}) \end{array} \quad \begin{array}{l} PSH^+\text{-}hypho\text{-8-R-8,13-}CNB_8H_{13}^- \\ (R = CH_3,\ \mathbf{5a}^-;\ \mathbf{5a}^-\text{-}^{13}C) \\ (R = Bn,\ \mathbf{5b}^-) \end{array} \qquad (12)$$

The ^{11}B NMR spectra of the anions (**5a**$^-$, **5b**$^-$, **5a**$^-$-^{13}C) show eight boron resonances. Their ^{1}H NMR spectra show resonances attributable to three bridge or endo hydrogens and the bridging −CH(R)NH= group. Based on their skeletal electron counts (n + 4 skeletal electron pairs), the **5**$^-$ anions would be the first 10-vertex hypho boron cages. The ab initio/IGLO/NMR calculations for **5a**$^-$ give good agreement with the experimental ^{11}B NMR chemical shifts (Table 1) for the hypho structure in Figure 17, which is derived from a 13-vertex closo polyhedron by removing the number 5, 7, and 11 vertices, as shown in Figure 18. Also, the calculated chemical shift assignments agree with the assignments determined by both the 2-D ^{11}B−^{11}B NMR spectrum of **5a**$^-$ and the ^{11}B{^{1}H} NMR spectrum of **5a**$^-$-^{13}C, which shows the expected ^{11}B−^{13}C coupling on the B3 resonance. The proposed structure of **5a**$^-$ can be generated from that of **4a**$^-$ by a cage degradation involving the loss of the B8 boron from **4a**$^-$ and addition of a bridge hydrogen on the B1−B2 edge.

The **5**$^-$ anion was reprotonated by HCl/Et_2O to regenerate **5** (eq 13), suggesting that they have the same 10-vertex hypho cage atom framework.

(26) (a) Greenwood, N. N.; Gysling, H. J.; McGinnety, J. A.; Owen, J. D. *J. Chem. Soc., Chem. Commun.* **1970**, 505−506. (b) Greenwood, N. N.; McGinnety, J. A.; Owen, J. D. *J. Chem. Soc., Dalton Trans.* **1972**, 986−989. (c) Huffman, J. C. Report No. 82210, Indiana University of Chemistry Molecular Structure Center.

(27) Schaeffer, R.; Sneddon, L. G. *Inorg. Chem.* **1972**, 11, 3102−3104.

(28) Williams, R. E. *Chem. Rev.* **1992**, *92*, 177−207 and references therein.

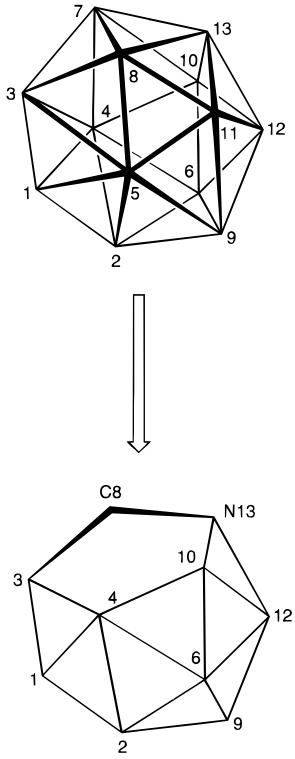

Figure 18. Derivation of the proposed 10-vertex hypho structures of **5** and **5**$^-$ from a 13-vertex closo polyhedron.

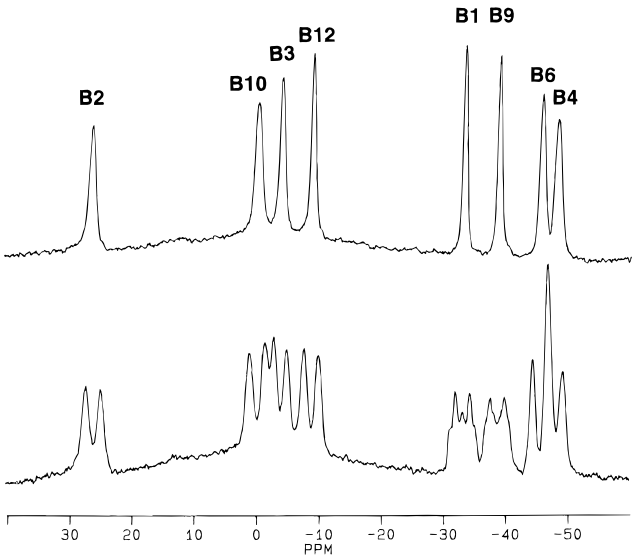

Figure 19. The 64.2-MHz ^{11}B NMR spectra of **5a**: (bottom) proton coupled and (top) proton decoupled.

$$\begin{array}{l} PSH^+\text{-}hypho\text{-8-R-8,13-}CNB_8H_{13}^- \xrightarrow[CH_2Cl_2]{H_2SO_4} \\ \quad (R = CH_3,\ \mathbf{5a}^-;\ \mathbf{5a}^-\text{-}^{13}C) \\ \quad\quad (R = Bn,\ \mathbf{5b}^-) \end{array} \quad \begin{array}{l} hypho\text{-8-R-8,13-}CNB_8H_{14} \\ (R = CH_3,\ \mathbf{5a};\ \mathbf{5a}\text{-}^{13}C) \\ (R = Bn,\ \mathbf{5b}) \end{array} \qquad (13)$$

Likewise, the assignments determined from the 2-D ^{11}B−^{11}B NMR spectrum of **5a** are consistent with the boron connectivities predicted for a boron framework similar to that proposed for **5a**$^-$. The ^{1}H{^{11}B} NMR spectrum shows, in addition to eight terminal BH resonances, four hydrogens at upfield chemical shifts, indicating bridge or endo hydrogens. The ^{11}B NMR spectrum of **5a** (Figure 19) shows eight boron resonances with

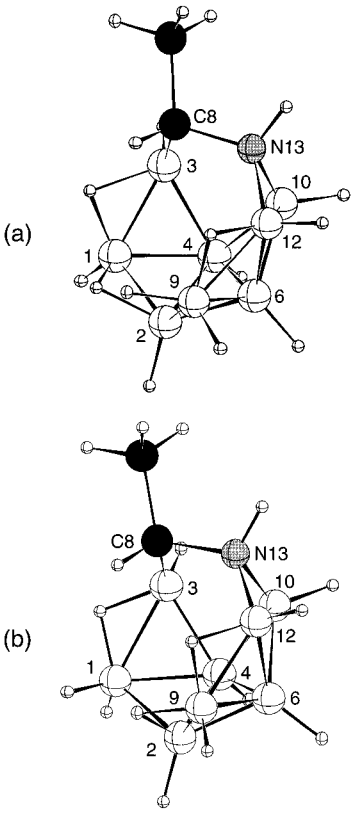

Figure 20. Comparison of the two calculated structures of **5a**.

triplet fine coupling observed on the resonances at −33.3 and −39.5 ppm, consistent with the coupling of each of these borons to two endo or bridge hydrogens.

The addition of a proton to the $\mathbf{5}^-$ anion could, in principle, occur at a number of places (Figure 17), including bridging positions at B2−B9, B9−B12, B3−B4, or B4−B10 or the endo positions at B1, B2, B12, or B4. In ab initio calculations, structures where the hydrogen was initially placed at the B2−B9 or B9−B12 edges or in the endo positions on the B1, B2, or B12 borons yielded the optimized structures shown in Figure 20. Addition of a proton at the B3−B4 or B4−B10 edges or at the endo-B4 position would result in an unfavorable[28] seven-coordinate boron and therefore, as expected, gave optimized structures that were much higher in energy. The two structures in Figure 20 have the same gross skeletal arrangement, and differ only in the location of two hydrogens. In structure (a), the two hydrogens are found at the B1−B2 edge and at the endo-B9 position, whereas in structure (b), the hydrogens are located at the B2−B9 edge and at the endo-B1 position. The two structures are close in energy with structure (a) being only ∼0.6 kcal/mol lower in energy than structure (b). The similar energies of these structures suggest that hydrogen migration about the B1−B2−B9 borons could readily occur in solution at room temperature. Indeed, interconversion between the two optimized structures can be envisioned to occur easily by moving the endo-B9 hydrogen on structure (a) to a bridging position on the B2−B9 edge, while moving the bridge hydrogen on the B1−B2 edge to the endo-B1 position. However, a more complex dynamic behavior is suggested by the fact that the IGLO calculated shifts of neither structure (a) or (b) gave good agreement with either the experimentally observed ^{11}B NMR chemical shifts or the assignments determined by the 2-D ^{11}B−^{11}B NMR experiments. Likewise, the resonance arising from the B3 boron directly attached to the carbon was experimentally determined (by the presence of 45 Hz ^{11}B−^{13}C coupling) in the NMR spectrum of **5a**-^{13}C to occur at −4.7 ppm, but this value falls between the IGLO calculated shifts for the two optimized structures: structure (a), B3, 2.1 ppm; structure (b), B3, −14.4 ppm. Thus, while the structure of the *hypho*-8-R-8,13-$CNB_8H_{13}^-$ anion would seem to be well established by the computational and experimental data, the exact structure of the neutral *hypho*-8-R-8,13-CNB_8H_{14} azamonocarbaborane must be considered unproven at this point.

In summary, the results discussed above have further demonstrated that a synthetic strategy involving nucleophilic attack of a polyhedral borane anion at a polar multiple bond provides a new route for the synthesis of hybrid cluster compounds unattainable by more conventional routes. Work is now in progress aimed at both expanding the scope of these reactions and exploring the chemical properties of these unique clusters.

Acknowledgment. We thank the National Science Foundation for the support of this research. We also thank Dr. Joe Barendt of Callery Chemical Co. for a gift of decaborane.

Supporting Information Available: Tables listing refined positional and thermal parameters, bond distances, bond angles, calculated atom positions, Cartesian coordinates, and calculated bond distances for the optimized geometries at the HF/6-31G* level for all of the systems calculated (56 pages). See any current masthead page for ordering and Internet access instructions.

JA960787M